



저작자표시-비영리-변경금지 2.0 대한민국

이용자는 아래의 조건을 따르는 경우에 한하여 자유롭게

- 이 저작물을 복제, 배포, 전송, 전시, 공연 및 방송할 수 있습니다.

다음과 같은 조건을 따라야 합니다:



저작자표시. 귀하는 원저작자를 표시하여야 합니다.



비영리. 귀하는 이 저작물을 영리 목적으로 이용할 수 없습니다.



변경금지. 귀하는 이 저작물을 개작, 변형 또는 가공할 수 없습니다.

- 귀하는, 이 저작물의 재이용이나 배포의 경우, 이 저작물에 적용된 이용허락조건을 명확하게 나타내어야 합니다.
- 저작권자로부터 별도의 허가를 받으면 이러한 조건들은 적용되지 않습니다.

저작권법에 따른 이용자의 권리는 위의 내용에 의하여 영향을 받지 않습니다.

이것은 [이용허락규약\(Legal Code\)](#)을 이해하기 쉽게 요약한 것입니다.

[Disclaimer](#)

Thesis for the Degree of Master of Physics

Investigations of the luminescence
properties of charge compensation on
 Bi^{3+} doped $\text{CaMoO}_4:\text{Eu}^{3+}$ phosphors



by

Eun Ock Kim

Department of Physics

The Graduate School

Pukyong National University

February 2015

Investigations of the luminescence
properties of charge compensation on
 Bi^{3+} doped $\text{CaMoO}_4:\text{Eu}^{3+}$ phosphors
(Bi^{3+} 가 첨가된 $\text{CaMoO}_4:\text{Eu}^{3+}$ 형광체의
전하보상에 의한 형광 특성 연구)

Advisor: Prof. Jung Hyun Jeong

by
Eun Ock Kim

A thesis submitted in partial fulfillment of the requirements
for the degree of

Master of Physics

Department of Physics, The Graduate School,
Pukyong National University

February 2015

Investigations of the luminescence properties of charge
compensation on Bi^{3+} doped $\text{CaMoO}_4:\text{Eu}^{3+}$ phosphors

A dissertation

by

Eun Ock Kim

Approved by:

Prof. Jung Hwan Kim
Chairman of Committee

Prof. Byung Kee Moon
Member of Committee

Prof. Jung Hyun Jeong
Member of Committee

December 2, 2014

Contents

Abstract.....vii

I. Introduction 1

II. Theoretical background 3

2.1 Luminescent materials 3

2.2 Luminescence mechanisms 6

2.2.1 Center Luminescence 7

2.2.2 Charge transfer mechanism 11

2.2.3 Energy transfer mechanism 12

2.3 Characteristics of rare earth ions 15

2.4 Luminescence property of Eu^{3+} ion 18

2.5 Luminescence property of Bi^{3+} ion 19

2.6 Structure of the CaMoO_4 20

2.7 Charge compensation condition 22

III. Experimental..... 23

3.1 Preparation of sample CaMoO_4 phosphors..... 23

3.1.1 Preparation of $\text{CaMoO}_4:\text{Eu}^{3+}$ phosphors..... 23

3.1.2 Preparation of $\text{CaMoO}_4:\text{Eu}^{3+}, \text{Bi}^{3+}$ phosphors 25

3.2 Characterization of the phosphors 25

IV. Results and discussions.....	29
4. 1 Effect of the charge compensation on Eu^{3+} doped CaMoO_4 phosphors	29
4.2 Luminescence properties of Eu^{3+} and Bi^{3+} co-doped CaMoO_4 phosphors	42
4.3 Effect of the charge compensation on luminescence properties of Eu^{3+} and Bi^{3+} co-doped CaMoO_4 phosphors.....	48
V. Conclusions	59
References.....	62

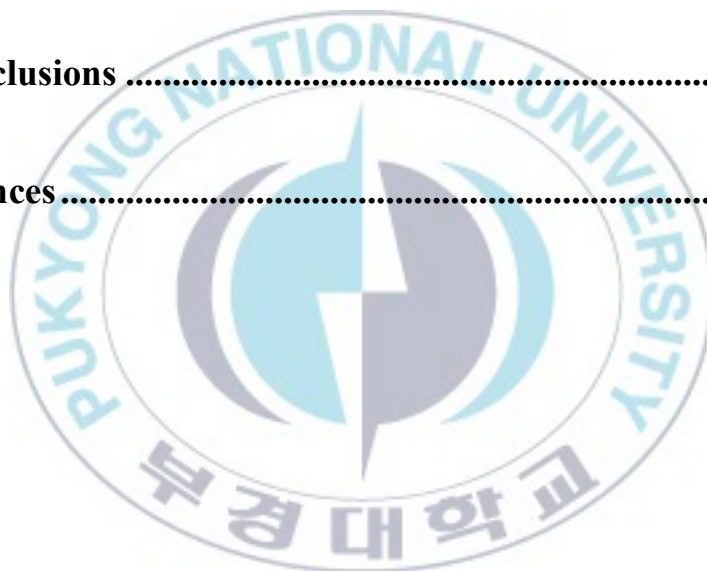


Table list

Table 2.1 Application of luminescence material	5
Table 2.2 Table of the basic properties of the trivalent rare earth elements	16
Table 4.1 Structural parameters of satisfied the charge compensation condition and otherwise	32
Table 4.2 The ${}^5D_0 \rightarrow {}^7F_2$ relative intensity of phosphors.....	58



Figure List

Figure 2.1 Schematic illustration of a luminescent material: (a) an activator ion A in its host lattice (Heat: nonradiative return to the ground strate) (b) energy transfer (ET) from a sensitizer S to an activator A	4
Figure 2.2 Schematic energy level scheme of luminescent material. Radiation and nonradiation indicated by R and NR, respectively	7
Figure 2.3 Schematic representation of the configurational coordination diagram	9
Figure 2.4 (a) Schematic energy level scheme of energy transfer between the S and A. (b) Schematic illustration of the spectral overlap at the bottom	14
Figure 2.5 Sketches of (a) electrostatic interaction; (b) exchange interaction, R, e, L denote distance between D and A, electron and effective Bohr radii, respectively	14
Figure 2.6 Illustration of the <i>Dieke diagram</i> : Energy levels of lanthanide ions	17
Figure 2.7 The crystal structure of CaMoO ₄ in the projection on the ac plane	21
Figure 3.1 Schematic diagram of the preparation process of CaMoO ₄ phosphors	24
Figure 3.2 X-ray diffractometer (X'PERT PRO, PHILIPS).....	27
Figure 3.3 Schematic representation of the photoluminescence system	28
Figure 4.1.1 (a) XRD patterns of uncompensated Ca _{0.95} MoO ₄ :0.05Eu ³⁺ and self-compensated Ca _{0.925} MoO ₄ :0.05Eu ³⁺ phosphors and the reference data of JCPDS card No. 07-0212, (b) enlarged XRD near 27-30° (2θ) for (1 1 2) main peak	31

Figure 4.1.2 Plot of $\beta\cos\theta$ against $4\sin\theta$ for $\text{Ca}_{0.95}\text{MoO}_4:0.05\text{Eu}^{3+}$ and $\text{Ca}_{0.925}\text{MoO}_4:0.05\text{Eu}^{3+}$ phosphors.....	32
Figure 4.1.3 SEM image of (a, c) uncompensated $\text{Ca}_{0.95}\text{MoO}_4:0.05\text{Eu}^{3+}$ and (b, d) compensated $\text{Ca}_{0.925}\text{MoO}_4:0.05\text{Eu}^{3+}$	35
Figure 4.1.4 PLE spectra of uncompensated $\text{Ca}_{0.95}\text{MoO}_4:0.05\text{Eu}^{3+}$ and compensated $\text{Ca}_{0.925}\text{MoO}_4:0.05\text{Eu}^{3+}$ phosphors by monitoring the emission wavelength at 617.5 nm.....	36
Figure 4.1.5 Gaussian fitting for PLE spectra of (a) uncompensated $\text{Ca}_{0.95}\text{MoO}_4:0.05\text{Eu}^{3+}$ and (b) compensated $\text{Ca}_{0.925}\text{MoO}_4:0.05\text{Eu}^{3+}$ phosphors.....	37
Figure 4.1.6 PL spectra of uncompensated $\text{Ca}_{0.95}\text{MoO}_4:0.05\text{Eu}^{3+}$ and compensated $\text{Ca}_{0.925}\text{MoO}_4:0.05\text{Eu}^{3+}$ phosphors under the excitation wavelength of 397.5 nm	39
Figure 4.1.7 Decay curves of (a) uncompensated $\text{Ca}_{0.95}\text{MoO}_4:0.05\text{Eu}^{3+}$ and (b) compensated $\text{Ca}_{0.925}\text{MoO}_4:0.05\text{Eu}^{3+}$ phosphors as a function of charge compensation	41
Figure 4.2.1 XRD patterns of $\text{Ca}_{0.95-x}\text{MoO}_4:0.05\text{Eu}^{3+}$, $x\text{Bi}^{3+}$ phosphors and the reference data of JCPDS card No. 07-0212	44
Figure 4.2.2 (a) PLE spectra of $\text{Ca}_{0.95-x}\text{MoO}_4:0.05\text{Eu}^{3+}$, $x\text{Bi}^{3+}$ phosphors by monitoring the emission wavelength at 617.5 nm and (b) Gaussian fitting for PLE spectra of $\text{Ca}_{0.94}\text{MoO}_4:0.05\text{Eu}^{3+}$, 0.01Bi^{3+} phosphors. The inset represents the effect of Bi^{3+} concentration at 397.5 nm.....	45
Figure 4.2.3 (a) 4.2.3 PL spectra of $\text{Ca}_{0.95-x}\text{MoO}_4:0.05\text{Eu}^{3+}$, $x\text{Bi}^{3+}$ with different concentration of Bi^{3+} ion under the excitation wavelength of 327.5 nm and (b) enlarged PL spectra near 400-600 (nm).....	47
Figure 4.3.1 XRD patterns of compensated $\text{Ca}_{0.925-1.5x}\text{MoO}_4:0.05\text{Eu}^{3+}$, $x\text{Bi}^{3+}$ phosphors and the reference data of JCPDS card No. 07-0212	49

Figure 4.3.2 (a) PLE spectra of $\text{Ca}_{0.925-1.5x}\text{MoO}_4:0.05\text{Eu}^{3+}, x\text{Bi}^{3+}$ phosphors by monitoring the emission wavelength at 617.5 nm and (b) Gaussian fitting for PLE spectra of $\text{Ca}_{0.91}\text{MoO}_4:0.05\text{Eu}^{3+}, 0.01\text{Bi}^{3+}$ phosphors. The inset represents the effect of Bi^{3+} concentration at 397.5 nm.	52
Figure 4.3.3 PL spectra of $\text{Ca}_{0.925-1.5x}\text{MoO}_4:0.05\text{Eu}^{3+}, x\text{Bi}^{3+}$ with different concentration of Bi^{3+} ion under the excitation wavelength of 334.5 nm	53
Figure 4.3.4 (a) XRD patterns of uncompensated $\text{Ca}_{0.94}\text{MoO}_4:0.05\text{Eu}^{3+}, 0.01\text{Bi}^{3+}$ and compensated $\text{Ca}_{0.91}\text{MoO}_4:0.05\text{Eu}^{3+}, 0.01\text{Bi}^{3+}$ phosphors, and the reference data of JCPDS card No. 07-0212, (b) enlarged XRD near $27-30^\circ$ (2θ) for (1 1 2) main peak	55
Figure 4.3.5 (a) PLE and (b) PL spectra of uncompensated $\text{Ca}_{0.94}\text{MoO}_4:0.05\text{Eu}^{3+}, 0.01\text{Bi}^{3+}$ and compensated $\text{Ca}_{0.91}\text{MoO}_4:0.05\text{Eu}^{3+}, 0.01\text{Bi}^{3+}$ phosphors	56
Figure 4.3.6 PL spectra of commercial of $\text{Y}_2\text{O}_3:\text{Eu}^{3+}$ and compensated $\text{Ca}_{0.91}\text{Eu}_{0.05}\text{Bi}_{0.01}\text{MoO}_4$ phosphors monitoring excitation wavelength at 397.5 nm	58

Investigations of the luminescence properties of charge compensation on

Bi^{3+} doped $\text{CaMoO}_4:\text{Eu}^{3+}$ phosphors

Eun Ock Kim

Department of Physics, The Graduate School

Pukyong National University

Abstract

When a metal ion is substituted for an element with a different valence in the matrix, charge compensation is needed. The charge compensation may cause to a vacancy (for example in this work; $3\text{Ca}^{2+} \rightarrow 2\text{Eu}^{3+} + \text{a calcium vacancy}$). Both of according to a charge compensation condition and without this condition, we have synthesized a series of $\text{CaMoO}_4:\text{Eu}^{3+}$ phosphors and Bi^{3+} co-doped in $\text{CaMoO}_4:\text{Eu}^{3+}$ phosphors.

A series of $\text{CaMoO}_4:\text{Eu}^{3+}$ phosphors satisfied with charge compensation condition were synthesized using the solid state reaction method. Comparing to uncompensated $\text{Ca}_{0.95}\text{MoO}_4:0.05\text{Eu}^{3+}$ phosphor, the crystallinity of compensated $\text{Ca}_{0.925}\text{MoO}_4:0.05\text{Eu}^{3+}$ phosphor is improved, and the lattice constant is increased. Also, CT band of $\text{Eu}^{3+} - \text{O}^{2-}$ and $\text{Mo}^{6+} - \text{O}^{2-}$ shifted towards the lower energy region due to the enhanced covalent bond interaction between the $\text{Eu}^{3+}/\text{Mo}^{6+}$ and

O²⁻ ions. The main emission of Ca_{0.925}Eu_{0.05}MoO₄ is ⁵D₀ → ⁷F₂ transition of Eu³⁺ at 617.5 nm, and emission intensity significantly increases about 3.7 times than that of uncompensated Ca_{0.95}Eu_{0.05}MoO₄.

A series of the Bi³⁺ co-doped in CaMoO₄:Eu³⁺ phosphors were fabricated to find out charge compensation with optimized. When Bi³⁺ ions are introduced to the phosphors, the self-absorption of Bi³⁺ from ground state (¹S₀) to the excited state (³P₁) in the wavelength range below 360 nm are observed. Besides, the oscillator strength of the electric dipole transitions from emitted Eu³⁺ in the sample including Bi³⁺ ions is increased about 2.6 – 4 times than that of undoped Ca_{0.95}MoO₄:0.05Eu³⁺. This is due to energy transfer from Bi³⁺ to Eu³⁺ and distortion of crystal field.

With the compensated Ca_{0.91}MoO₄:0.05Eu³⁺, 0.01Bi³⁺ phosphor, it occur the increasing intensity of excitation and emission compared with uncompensated Ca_{0.94}MoO₄:0.05Eu³⁺, 0.01Bi³⁺. The emission intensity is increased about 2.5 times than uncompensated Ca_{0.94}MoO₄:0.05Eu³⁺, 0.01Bi³⁺. The result indicates that appropriate dopant of Bi³⁺ ions is related with charge compensation. Of these materials, Ca_{0.91}MoO₄:0.05Eu³⁺, 0.01Bi³⁺ exhibits the strongest red emission. The integral emission intensity of Ca_{0.91}MoO₄:0.05Eu³⁺, 0.01Bi³⁺ phosphor under excitation wavelength of 397.5 nm is about 3.4 times higher than that of commercial Y₂O₃:Eu³⁺ phosphor.

I. Introduction

At present, white light-emitting diodes (WLEDs) have become a highly popular and competitive light source as third generation lighting sources [1-3]. They have attracted substantial attention owing to their extraordinary luminescence efficiency, low power consumption, high brightness and environmental protection [3-5].

Generally, Eu^{3+} -doped phosphors are considered as the red emission source needed to improve the color-rendering index in WLEDs. Eu^{3+} is a preferable choice, because Eu^{3+} ions located in a site with low symmetry and which have strong covalent interaction between the activator and the surrounding anions [6-9]. In particular, it can be emit high purity color of the red light due to ${}^5\text{D}_0 \rightarrow {}^7\text{F}_2$ transition at a low symmetry site [8,9]. Many scheelite-type structure phosphors doped with Eu^{3+} have been studied extensively. In the scheelite structure, molybdate (MoO_4^{2-}) is a good choice as a host material because of their excellent optical and physical properties such as great strength, chemical and thermal stability, high decomposition temperature [6,10-14].

Recently, the energy transfer from a sensitizer Bi^{3+} to an activator Eu^{3+} has been reported in several hosts [7,15-19]. In particular, much attention is focused on the improvement of luminescent properties of molybdate phosphors co-doped of Bi^{3+} ions [18,19]. It is well known that Bi^{3+} ion are as an activator as well as a sensitizer of luminescence. It can be efficiently enhanced the luminescence intensity compared to the single Eu^{3+} doped phosphor hosts. In addition, Bi^{3+} ion

is a post-transition metal ion with $6s^2$ configuration, which consists of a strong broad absorption in the UV region due to $^1S_0 \rightarrow ^3P_0$ transition. And the Bi^{3+} emission is known to cover a very broad spectral range from the UV to the red depending on the host lattice [20,21].

In the present study, phosphors are synthesized without any charge compensation of ions [10-12,14]. But, when a metal ion is substituted for an element with a different valence in the matrix, charge compensation is needed. As reported by Liu et al [13] $\text{CaMoO}_4:\text{Eu}^{3+}$ discussed the effect of different charge compensation that using ions such as K^+ , Na^+ , Li^+ , and found that efficient charge compensation could enhance the luminescence intensity. In this research, the luminescent properties of the phosphor were studied, in which different charge compensation approaches are applied. And, the influence of Bi^{3+} incorporation on the structural and luminescence properties of $\text{CaMoO}_4:\text{Eu}^{3+}$ should be investigated in detail.

II. Theoretical background

2.1 Luminescent materials

Luminescent materials (or phosphors) are a solid which converts certain types of energy into electromagnetic radiation over and above thermal radiation. The electromagnetic radiation emitted by a luminescent material is usually in the visible range, but can also be in other spectral regions, such as the ultraviolet or infrared. Luminescence can occur as a result of many different kind of energy, and photoluminescence is excited by electromagnetic (often ultraviolet) radiation, cathodoluminescence by a beam of energetic electrons, electroluminescence is excited by an electric voltage, triboluminescence is excited by mechanical energy (e.g. grinding), X-ray luminescence is excited by X-ray, chemiluminescence is excited by the energy of a chemical reaction, and so on as shown in Table. 2.1.

Luminescence materials are mostly solid inorganic materials consisting of a host lattice, usually intentionally doped with activator ions. In order to illustrate the definition of a luminescent material, it has been drawn schematically in Fig. 2.1(a). For example, consider the famous luminescent materials $\text{Al}_2\text{O}_3:\text{Cr}^{3+}$ and $\text{Y}_2\text{O}_3:\text{Eu}^{3+}$. The host lattices are Al_2O_3 and Y_2O_3 , the activators the Cr^{3+} and Eu^{3+} ions. When the activator ions show too weak an absorption, a second kind of impurities can be added (sensitizer), which absorb the exciting radiation and subsequently transfer it to the activator. This process involves transport of energy through the luminescent materials. For example, $\text{Ca}_5(\text{PO}_4)_3\text{F}:\text{Sb}^{3+},\text{Mn}^{2+}$. Ultra violet radiation is not absorbed by Mn^{2+} , but only by Sb^{3+} . Under ultraviolet

irradiation, the emission consists partly of blue Sb^{3+} emission, and partly of yellow Mn^{2+} emission. Since the Mn^{2+} ion was not excited directly, the excitation energy was transferred from Sb^{3+} to Mn^{2+} in shown Fig. 2.1(b) [22].

Luminescent materials are generally made out of a suitable host material in combination with an activator. Most of these materials are oxides, nitrides and oxynitrides, silicates and various rare earth metals doped with transition metal ions or rare-earth ions.

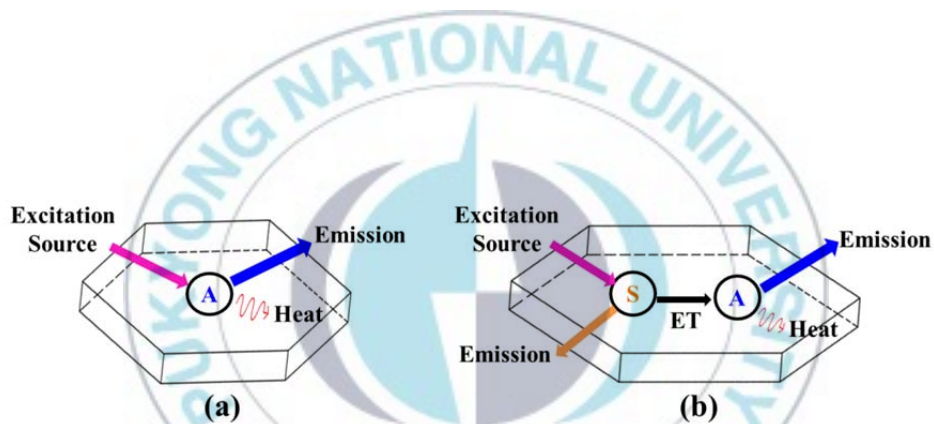


Figure 2.1 Schematic illustration of a luminescent material: (a) an activator ion A in its host lattice (Heat: nonradiative return to the ground state) (b) energy transfer (ET) from a sensitizer S to an activator A .

Table 2.1 Application of luminescence material [23,24].

Energy source	Excitation energy	Application
	250-400 nm	High pressure mercury lamp
	254 nm	Fluorescence lamp
Photoluminescence		Phosphor-converted Light
	380 nm	Emitting Diode
	147 nm	Plasma Display Panel
Cathode-Luminescence	Cathode Ray	Cathode Ray Tube
		Field Emission Display
		Vacuum Fluorescence Display
Electroluminescence	Electric Field	Organic Light Emitting Diodes
		Light Emitting Diode
Chemiluminescence	Chemical reaction energy	Emergency lighting, glow sticks, blood detection, etc.
X-rays luminescence	X-rays	X-rays intensifier

2.2 Luminescence mechanisms

The luminescence in materials usually involves the following processes: (1) excitation of the activator to a higher energy state, (2) relaxation of the activator ion to the lowest energy level of the excited state, and (3) emission of a lower energy photon as the activator ion returns from its excited state to the ground state. The lifetime of emission transitions is ranged from 10^{-9} to 10 s [2,22].

The details of these processes can be explained by Fig. 2.2. The incident radiation is absorbed by the activator, raising it to an excited state. The excited ion returns to the ground state after emission of radiation or non-radiative decay. The nonradiative energy can be used to excite the vibrations of the host lattice. It is necessary to avoid the non-radiative process in order to enhance the luminescent material efficiently. Sometime excitation radiation is absorbed by the sensitizer ions, and subsequently transferred to the active ions. In many cases the host lattice transfers its excitation energy to the activator. In this case, the host lattice acts as the sensitizer. High-energy excitation always excites the host lattice. Direct excitation of activator is only possible with ultraviolet and visible radiation [23].

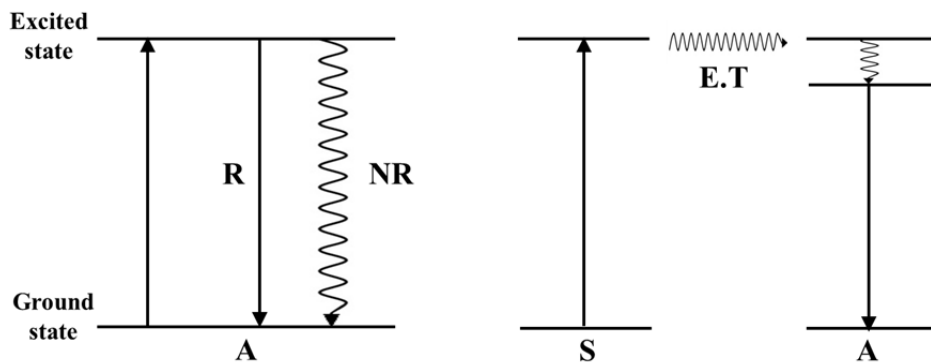


Figure 2.2 Schematic energy level scheme of luminescent material. Radiation and nonradiation indicated by *R* and *NR*, respectively [22].

2.2.1 Center Luminescence

In the case of center luminescence, the emission is generated on an optical center, in contradiction to, e.g., emission, which results from optical transitions between host lattice band states or from a transition between two centers. Such an optical center can be an ion or a molecular ion complex. One speaks of characteristic luminescence when, in principle, the emission could also occur on the ion in a vacuum, i.e. when the optical transition involves electronic states of the ion only. Characteristic luminescence possess a relatively sharp emission bands (spectral width of few nm, typically), but also of broad bands, which can have widths exceeding 50 nm in the visible part of the spectrum. Broad emission bands are observed when the nature of the chemical bonding in the ground and excited state differs considerably. This occurs simultaneously with a change in

equilibrium distance between the emitting ion and its immediate chemical environment and is better explained with the configuration coordinate diagram [24].

Fig 2.3 shows a configuration coordinate diagram where E is plotted versus R . Consider first the curve for the lowest, the ground state. Its shape is parabolic with a minimum at R_0 . Transitions between two parabolas are electronic transitions. In principle, consider to the interaction between the electrons and the vibrations of the optical center. Actually the value of $\Delta R = R'_0 - R_0$ is a qualitative measure of this interaction.

In optical absorption the center is promoted from its ground state to an excited state. It is important to realize that optical transitions occur in this diagram as vertical transitions. The reason for this is that a transition from the ground state to the excited state is electronic, whereas horizontal displacements in this diagram are nuclear, the distance R being an internuclear distance. Since the electrons move much faster than the nuclei, the electronic transition takes, in good approximation, place in static surroundings.

The optical absorption transition starts from the lowest vibrational level, i.e. $\nu = 0$. Therefore, the most probable transition occurs at R_0 where the vibrational wave function has its maximum value. The transition will end on the edge of the excited state parabola, since the vibrational levels of the excited state have their highest amplitude. This transition corresponds to the maximum of the absorption band. When $\Delta R = 0$, the vibrational overlap will be maximal for the levels $\nu = 0$ and $\nu' = 0$, since the vibrational wave function involved have their maximum at

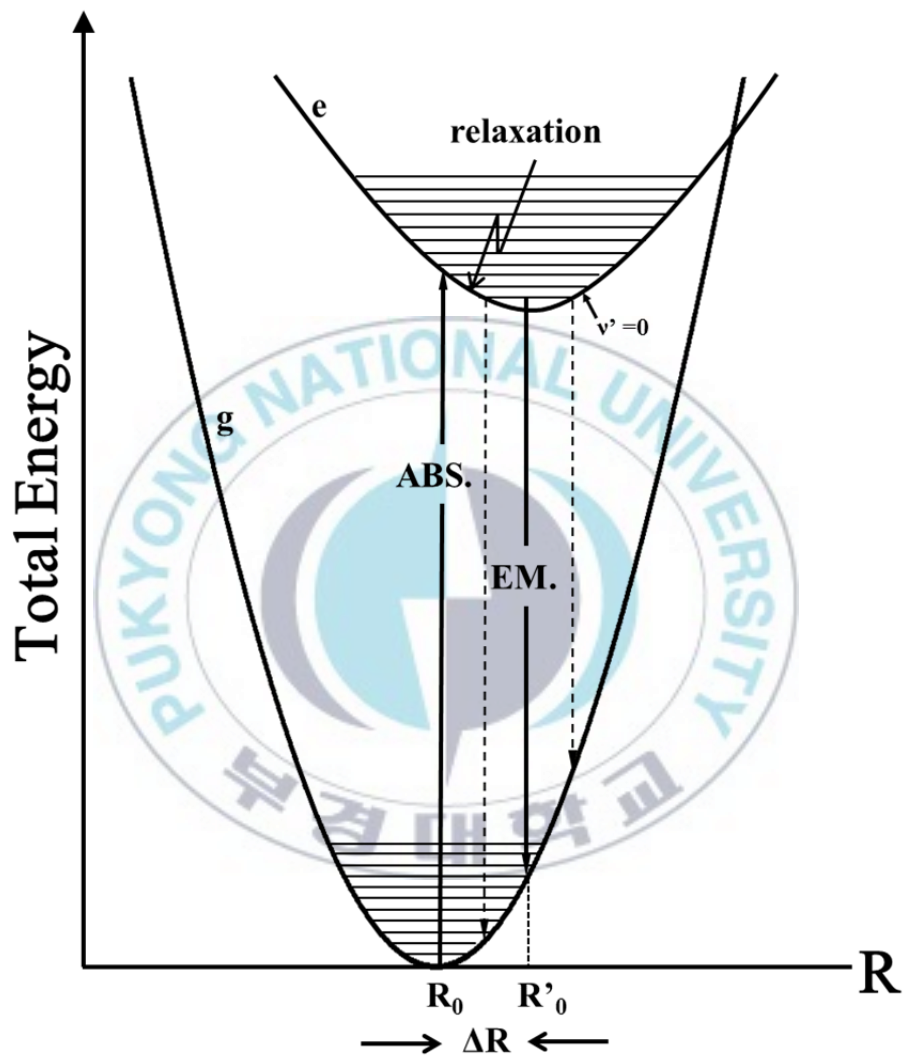


Figure 2.3 Schematic representation of the configurational coordination diagram [8,22].

the same value of R , viz. R_0 . The absorption spectrum consists of one line, corresponding to the transition from $\nu = 0$ to $\nu' = 0$. This transition is called the zero-vibrational or no-phonon transition, since no vibrations are involved. However, if $\Delta R \neq 0$, the $\nu = 0$ level will have the maximal vibrational overlap with several levels $\nu' > 0$, and a broad absorption band is observed.

The broader the absorption band, the larger the value of ΔR . The width of an absorption band informs us the difference in ΔR between the excited state and the ground state.

It is usual to call the $\Delta R = 0$ situation the weak-coupling scheme, $\Delta R > 0$ the intermediate-coupling scheme, and $\Delta R \gg 0$ the strong-coupling scheme. The word coupling relates to the coupling between the electrons and the vibrations of the center considered. The value of ΔR measures the strength of this interaction.

From the lowest vibrational level of the excited state the system can return to the ground state spontaneously under emission of radiation. The rules for this process are the same as described for the absorption process. The difference is that emission occurs spontaneously, whereas absorption can only occur when a radiation field is present.

By emission, the center reaches a high vibrational level of the ground state. Again relaxation occurs, but now to the lowest vibrational level of the ground state. The emission occurs at a lower energy than the absorption due to the relaxation processes in Fig .2.3. The energy difference between the maximum of the excitation band and emission band is called the Stokes shift. The value of ΔR is the Stokes shift.

If the two parabolas have equal force constants, the amount of energy lost in the relaxation process is $S\hbar\nu$ per parabola, where $\hbar\nu$ is the spacing between two vibrational levels and S an integer. The Stokes shift amounts to $2S\hbar\nu$. The constant S is called the Huang-Rhys coupling constant. It is proportional to $(\Delta R)^2$ and measures the strength of the electron-lattice coupling. If $S < 1$, is in the weak-coupling regime, if $1 < S < 5$, in the intermediate coupling regime, if $S > 5$, in the strong-coupling regime [22].

2.2.2 Charge transfer mechanism

The transfer of an electron from the ligand to the central metal ion is known as charge transfer transition. In the case of charge transfer, the optical transition takes place between different kinds of orbitals or between electronic states of different ions. The charge distribution on the optical center is very strongly changed by such an excitation. Consequently, the chemical bonding is significantly changed. In these cases, very broad emission spectra are expected. Selection rules for electromagnetic transition are loosened because charge transfers in initial and final states are different.

A very well-known example is CaWO_4 , used for decades for the detection of X-rays, which shows luminescence originating from the $(\text{WO}_4)^{2-}$ group. A similar compound, also showing blue emission, was used in early generations of fluorescent lamps: MgWO_4 . The transition involves charge transfer from oxygen ions to empty d-levels of the tungsten ion.

Several examples of charge transfer transitions have been given above. These were all of the LMCT (ligand to metal charge transfer) type. However, MLCT (metal to ligand charge transfer) is also possible, although in oxides not very probable. In coordination compounds these are quite common.

2.2.3 Energy transfer mechanism

Consider two centers, S and A , separated in a solid by distance R , and the energy level schemes are also given in Fig. 2.4(a). An asterisk indicates the excited state. Energy transfer between a sensitizer ion (S) and an activator ion (A) can be written as a chemical reaction: $S^* + A \rightarrow S + A^*$.

It is assumed that the distance R is so short that the centers S and A have a non-vanishing interaction with each other. If S is in the excited state and A in the ground state, the relaxed state of S may transfer its energy to A [22].

For energy transfer, the sensitizer ion and the activator ion have to show physical interaction. This energy transfer can find its origin in electrostatic and exchange interaction. The electrostatic interaction, it appears to be coulomb interaction, be described by Förster mechanism, and exchange interaction be described by Dexter mechanism. Sketches of the two types of interaction for resonant energy transfer are depicted in Fig. 2.5. In addition, the emission spectrum of the sensitizer ion and the absorption spectrum of the activator ion have to show spectral overlap, for energy conservation reasons in Fig 2.4(b).

The distance dependence of the transfer rate depends of the type of

interaction. For electric multipolar interaction the distance dependence is given by R^{-n} ($n = 6, 8, 10$ for electric dipole – electric dipole (d-d) interaction, electric dipole – electric quadrupole (d-q) interaction, electric quadrupole – electric quadrupole (q-q) interaction, respectively). Electric multipolar interaction is favored by a large spectral overlap, a small value of the intrinsic decay time of the sensitizer ion, large absorption strength of the activator ion, and a small distance between the sensitizer and activator ion [24].

When S and A are close enough and their wave-functions are overlapped, the energy transfer mechanism from S to A can be exchange interaction. For exchange interaction the distance dependence is exponential, since exchange interaction wave function overlap. The exponential dependence is due to the fact that the electron density in general falls off exponentially with the distance between the electron and the nucleus. In the case of energy transfer by exchange interaction, the rate drops very quickly for distances R_{SA} greater than about 1 nm. Finally, exchange interaction has an angular dependency, and depends on the covalence. This is because the wave function overlap is required.

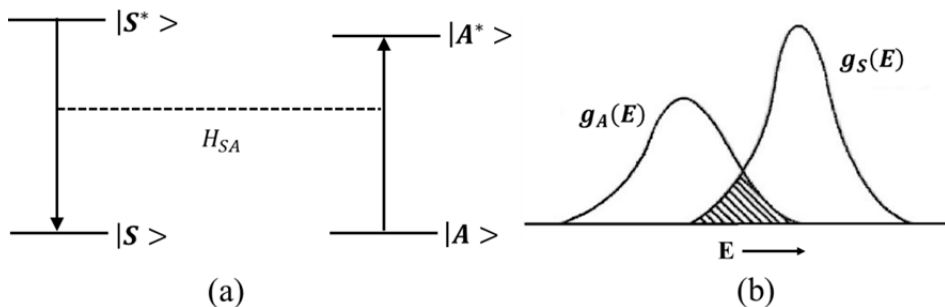


Figure 2.4 (a) Schematic energy level scheme of energy transfer between the S and A . (b) Schematic illustration of the spectral overlap at the bottom [22].

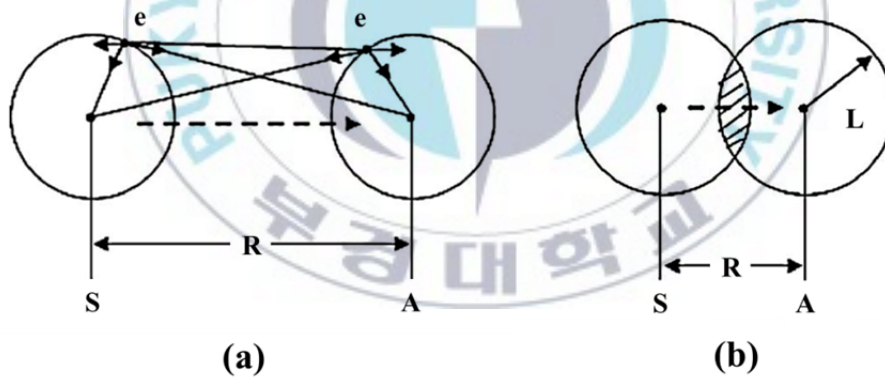


Figure 2.5 Sketches of (a) electrostatic interaction; (b) exchange interaction, R , e , L denote distance between D and A , electron and effective Bohr radii, respectively [8].

2.3 Characteristics of rare earth ions

The rare earth (RE) is the common name for 17 elements consisting of the 15 Lanthanides from Lanthanum to Lutetium, of Scandium, and of Yttrium. They have atomic numbers 21, 39 and from 57 to 71 in the Periodic table. The electronic configurations of trivalent rare-earth ions in the ground state and the ionic radius R (in coordination number (CN) = 8) of trivalent rare-earth ions are shown in Table 2.2. The $4f$ orbital of Lanthanides are shielded due to the surroundings environment by the filled $5s^2$ and $5p^6$ orbital. The partially filled $4f$ orbital is responsible for the characteristic optical and magnetic properties of the lanthanides.

The characteristic energy levels of $4f$ orbital of trivalent lanthanide ions have been precisely carried out by Dieke and co-workers in his 1968 book [25]. The characteristic energy levels of trivalent lanthanide ions are illustrated in Fig. 2.6, which is known as a “Dieke diagram”. As divalent ions, RE elements exhibit broad absorption-emission lines related to allowed $4f \rightarrow 5d$ transitions. In the trivalent form, RE elements lose two $6s$ electrons and one $4f$ or $5d$ electron [26,27]. Many of these ions can be used as luminescent ions in phosphors, mostly by replacing Y^{3+} , Gd^{3+} , La^{3+} and Lu^{3+} in various compound crystals.

Table 2.2 Table of the basic properties of the trivalent rare earth elements [28].

Atomic number	Name of the Ion	4f electronic Configuration	Ground state	R (Å)
57	La ³⁺	4f ⁰	¹ S ₀	1.16
58	Ce ³⁺	4f ¹	² F _{5/2}	1.143
59	Pr ³⁺	4f ²	³ H ₄	1.126
60	Nd ³⁺	4f ³	⁴ I _{9/2}	1.109
61	Pm ³⁺	4f ⁴	⁵ I ₄	1.093
62	Sm ³⁺	4f ⁵	⁶ H _{5/2}	1.097
63	Eu ³⁺	4f ⁶	⁷ F ₀	1.066
64	Gd ³⁺	4f ⁷	⁸ S _{7/2}	1.053
65	Tb ³⁺	4f ⁸	⁷ F ₆	1.04
66	Dy ³⁺	4f ⁹	⁶ H _{15/2}	1.027
67	Ho ³⁺	4f ¹⁰	⁵ I ₈	1.015
68	Er ³⁺	4f ¹¹	⁴ I _{15/2}	1.004
69	Tm ³⁺	4f ¹²	³ H ₆	0.994
70	Yb ³⁺	4f ¹³	² F _{7/2}	0.985
71	Lu ³⁺	4f ¹⁴	¹ S ₀	0.977

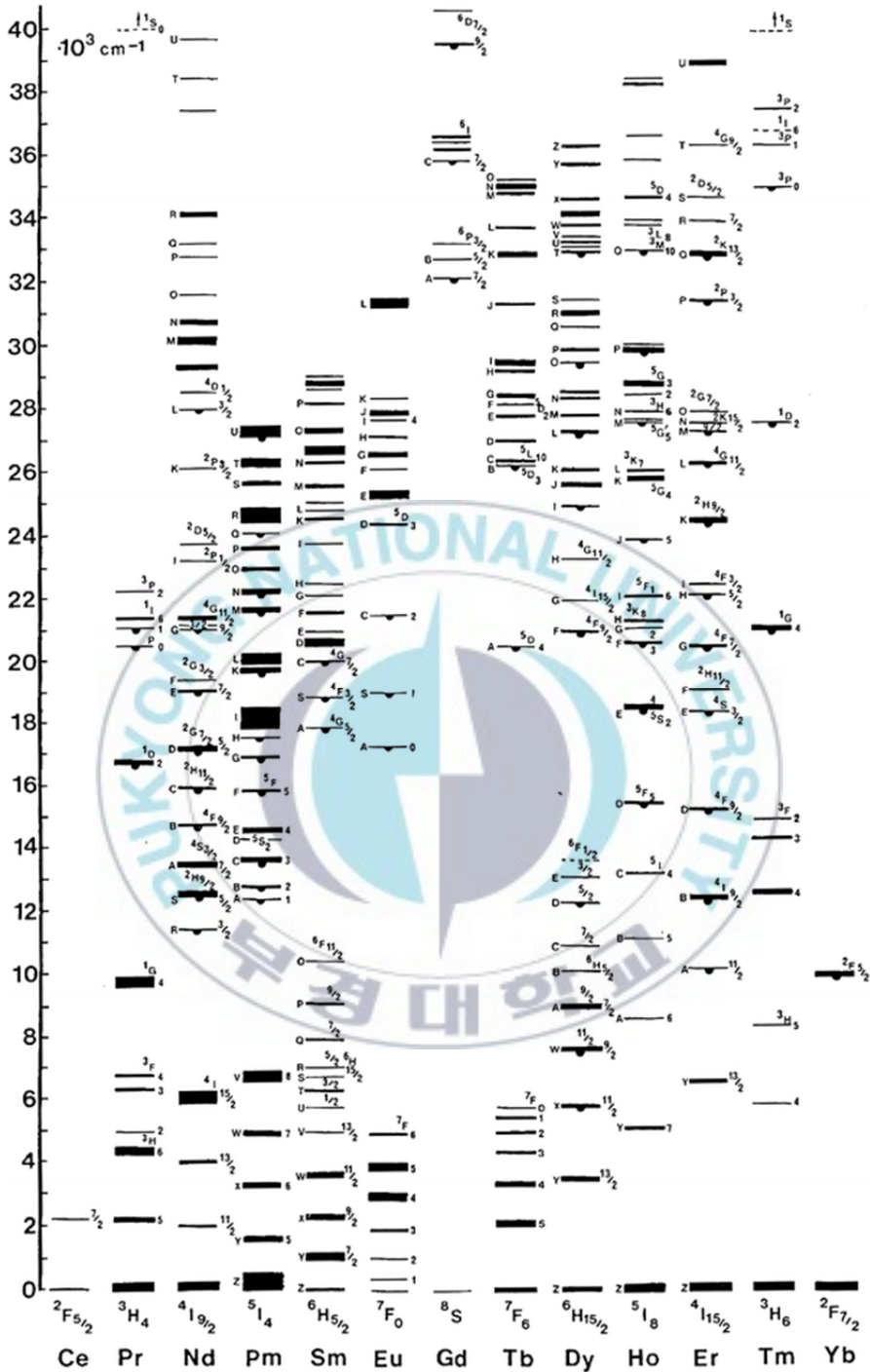


Figure 2.6 Illustration of the *Dieke diagram*: Energy levels of lanthanide ions

[25].

2.4 Luminescence property of Eu^{3+} ion

Eu^{3+} (f^6) has been used in most commercial red phosphors as an activator ion with red emission via ${}^5\text{D}_0 \rightarrow {}^7\text{F}_2$ transition at about 613 nm. The emission in the vicinity of 600 nm is due to the magnetic dipole transition of ${}^5\text{D}_0 \rightarrow {}^7\text{F}_1$, while the emission around 610 ~ 630 nm is due to the electric dipole transition of ${}^5\text{D}_0 \rightarrow {}^7\text{F}_2$. The intensity of electric dipole transitions depends strongly on the site symmetry in the lattice, whereas the magnetic dipole $f-f$ transitions are not affected much by the site symmetry because they are parity-allowed. If rare earth ion in the crystal lattice occupies a site with inversion symmetry, optical transitions between the $4f$ level are strictly forbidden as electric dipole transitions (parity selection rule). If the Eu^{3+} ion occupies the site without inversion symmetry, the electric dipole transitions are no longer strictly forbidden. And the intensity of the electric dipole emission is stronger than that of the magnetic dipole emission. Luminescent Eu^{3+} ions in commercial red phosphors such as YVO_4 , Y_2O_3 and $\text{Y}_2\text{O}_2\text{S}$, occupy the sites that have no inversion symmetry [8,29].

The spectral luminous efficacy as sensed by the eye has its maximum at 555 nm. In the red region, this sensitivity drops rapidly as one move toward longer wavelengths. Therefore, red luminescence composed of narrow spectra appear brighter to the human eye than various broad red emissions having the same red chromaticity and emission energy. For the red emission of color TV to be used in the NTSC system, the red chromaticity standard has been fixed at the coordinates $x = 0.67$, $y = 0.33$; in 1955, the ideal emission spectra were proposed as a narrow

band around 610 nm, before the development of Eu^{3+} phosphors. Use of narrow-band luminescence is also advantageous in three-band fluorescent lamp applications, where both brightness and color reproducibility are required. $\text{Y}_2\text{O}_3:\text{Eu}^{3+}$ has been used as the red-emitting component as a high color rendering lamp.

2.5 Luminescence property of Bi^{3+} ion

The trivalent bismuth ion (Bi^{3+}) is an interesting luminescence activator or sensitizer for phosphors due to electron transitions between the $6s^2$ ground state and the $6s^16p^1$ excited states [30]. We know that (1) the ground state (1S_0) of the isolated Bi^{3+} ion has a $6s^2$ configuration and (2) electronic transition to a $6s^16p^1$ configuration raise the excited states of triplet levels ($^3P_{0,1,2}$) and the 1P_1 singlet state. The lowest energy $^1S_0 \rightarrow ^3P_0$ transition is strongly forbidden, but the $^1S_0 \rightarrow ^3P_1$ transition (A-band) and the $^1S_0 \rightarrow ^3P_2$ transition (B-band) become more allowed due to spin-orbit coupling and coupling to asymmetrical phonon modes, respectively. The $^1S_0 \rightarrow ^1P_1$ transition (C-band) is an allowed electric dipole transition. Typically at room temperature, emission is observed from the $^3P_1 \rightarrow ^1S_0$ transition, although at low temperatures the highly forbidden $^3P_0 \rightarrow ^1S_0$ emission is also observed [31].

The Bi^{3+} emission is observed to cover a very broad spectral range, extending from the UV to the red. The broad luminescence band shows a strong

dependence on the composition and crystal structure of the host lattice because the outer electron orbital of Bi^{3+} are not shielded (as in the case of the $4f$ energy levels of trivalent lanthanide ions). Thus, emission wavelength is tunable from the ultraviolet, through blue to green [30,32].

2.6 Structure of the CaMoO_4

CaMoO_4 is one of the most important materials among the metal molybdate families, which have a high application potential in various fields, such as in photoluminescence, microwave applications and electro-optic applications [33,34]. The molybdenum (Mo^{6+}) atom adopts a tetrahedral coordination with oxygen ligands, while bivalent metal atoms have polyhedral coordination as shown in Fig. 2.7. Furthermore, MoO_4^{2-} tetrahedron exhibits efficiently strong absorption in the near-UV region and energy transfer the absorbed energy to the doping centers [12,35]. It is related to the charge transfer (CT) from oxygen to molybdenum ($2p \rightarrow 4d$ orbital) in the MoO_4^{2-} tetrahedron [36].

Among the scheelite structured materials, especially, CaMoO_4 is the most famous optical material, which has attracted much due to its importance in applications as a laser host material in quantum electronics or scintillators. In addition, the scheelite-type structured CaMoO_4 has been the subject of numerous investigations on its luminescent properties. Moreover, CaMoO_4 reflects its intriguing features include a high melting points (1445-1480 °C), effective

average decay time (14 μ s), refractive index (1.98), photoelectron yield (9%), non-hygroscopic, higher thermal, chemical and mechanical stabilities [37,38].

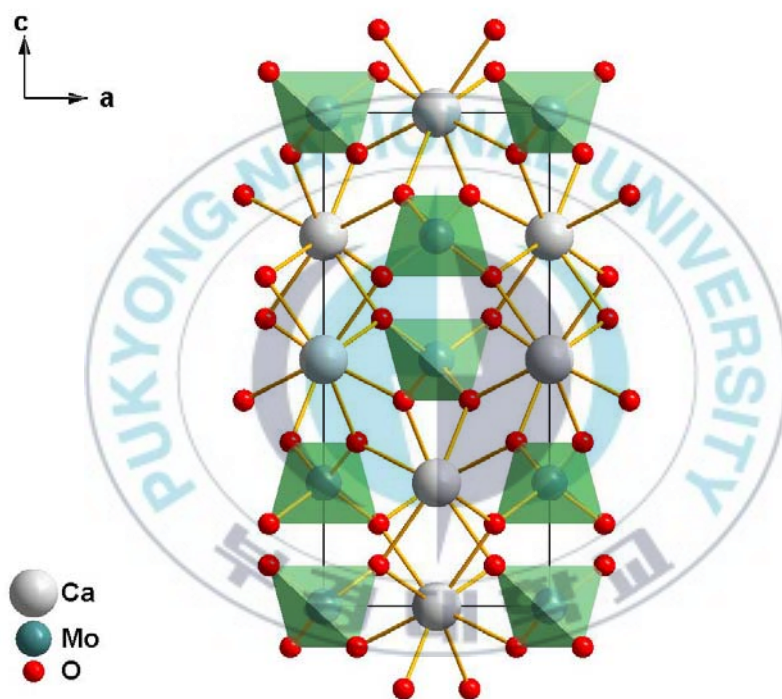


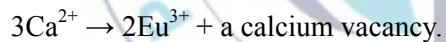
Figure 2.7 The crystal structure of CaMoO_4 in the projection on the ac plane.

2.7 Charge compensation condition

In CaMoO_4 phosphors, one Ln^{3+} ion is replaced by one Ca^{2+} ion. It would be difficult to keep charge compensation in the phosphor. It needs extra O^{2-} ions at nearby interstitial position. Defect leads to the distortion of local environment symmetries of optical centers. So, the host has to capture O^{2-} in the air to solve the problem. Therefore, an occurrence of more than just one Ln^{3+} site in the crystal lattice is anticipated [39-42]. The charge compensation can most probably be achieved by two possible mechanisms: (a) two Ca^{2+} ions are replaced by one Eu^{3+} ions and one monovalent cations.



Where, M^+ is a monovalent cation like Li^+ , Na^+ and K^+ acting as a charge compensator; (b) the charge compensation is provided by a calcium vacancy



III. Experimental

3.1 Preparation of sample CaMoO_4 phosphors

The solid state reaction is known as the most simple and basic preparation method, and has the obvious advantage of simplicity. This method has been widely used as method for the preparation of polycrystalline solids from a mixture of oxides, (oxy)nitrides, and fluorides because it is simple and very suitable for mass production. The planetary ball mill is introduced to improve the process of conventional solid state reaction, and is affected by the impact of grinding balls. The powder material is finely milled and well mixed through the motion of a grinding bowl.

The CaMoO_4 phosphors were prepared by solid state reaction using the planetary ball mill. The schematic diagram for the preparation has been presented in Fig. 3.1. A planetary ball mill was operated 10 times at a rotation speed of 350 rpm for 50 min with an interruption time of 10 min.

3.1.1 Preparation of $\text{CaMoO}_4:\text{Eu}^{3+}$ phosphors

A series of $\text{CaMoO}_4:\text{Eu}^{3+}$ phosphors related with charge compensation were synthesized using the solid state reaction method. $\text{Ca}_{1-x}\text{MoO}_4:\text{xEu}^{3+}$ and $\text{Ca}_{1-1.5x}\text{MoO}_4:\text{xEu}^{3+}$ ($x=0.05$ mol) precursor powders by molar ratio formula was prepared by taking stoichiometric amount of calcium carbonate (CaCO_3 , 99.95%, Aldrich), molybdenum oxide (MoO_3 , 99.5%, Aldrich), europium oxide (Eu_2O_3 ,

99.99%, Aldrich). All the prepared reagents were grinded by the planetary ball mill. And then, the mixed powders were firstly pre-fired at 600°C for 3 h, and then at 900 °C for 3h in air.

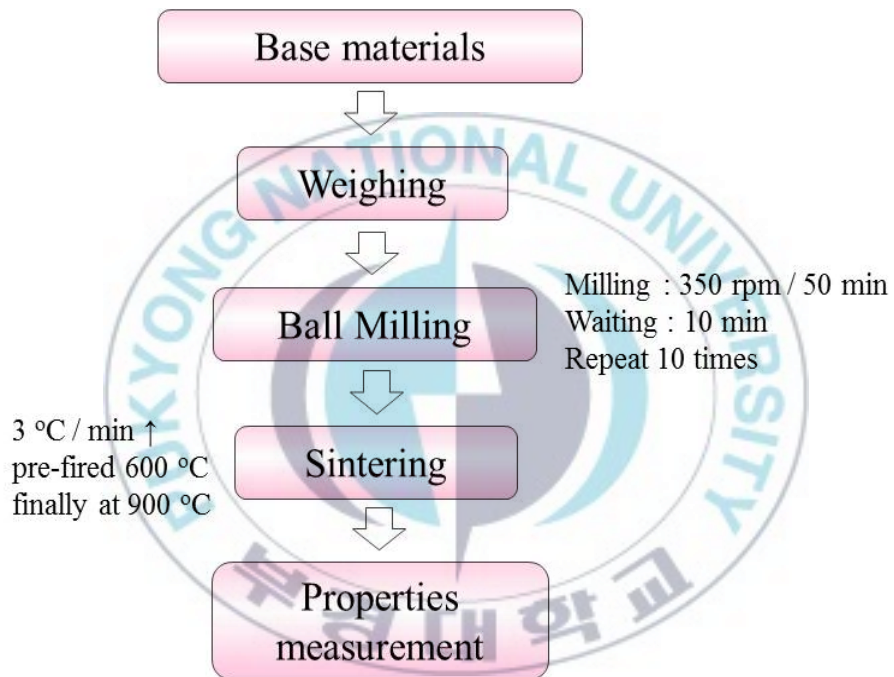


Figure 3.1 Schematic diagram of the preparation process of CaMoO_4 phosphors.

3.1.2 Preparation of $\text{CaMoO}_4:\text{Eu}^{3+}$, Bi^{3+} phosphors

Also, a series of $\text{CaMoO}_4:\text{Eu}^{3+}$, Bi^{3+} co-doped with different concentrations phosphors involved in charge compensation were synthesized using the solid state reaction method. $\text{Ca}_{1-x-y}\text{MoO}_4:\text{xEu}^{3+}$, yBi^{3+} and $\text{Ca}_{1-1.5(x+y)}\text{MoO}_4:\text{xEu}^{3+}$, yBi^{3+} ($x=0.05$, $y=0$, 0.005 , 0.01 , 0.02 , 0.03 mol) precursor powders by molar ratio formula was prepared. After the prepared mixture of CaCO_3 (99.95%, Aldrich), MoO_3 (99.5%, Aldrich), Eu_2O_3 (99.99%, Aldrich), and Bi_2O_3 (99.99%, Aldrich) were grinded by the planetary ball mill. And then, the powders sintered at same temperature.

3.2 Characterization of phosphors

The phosphors were characterized by X-Ray Diffractometer (XRD), Field Emission Scanning Electron Microscopy (FE-SEM) and Photoluminescence spectrophotometer with decay curves measurement, respectively

For determination of crystal structure and lattice parameter, samples were investigated by X-ray diffractometer (XRD). The XRD profiles were measured within the range of $10\text{-}70^\circ$ in steps of 0.02° using X-ray diffractometer (X'PERT PRO, PHILIPS) with $\text{CuK}_\alpha = 1.5406 \text{ \AA}$ radiation at 40 kV and 30 mA as shown in Fig. 3.2. The data obtained from the XRD were compared with the Joint Committee Powder Diffraction Standard (JCPDS) cards and the unit cell

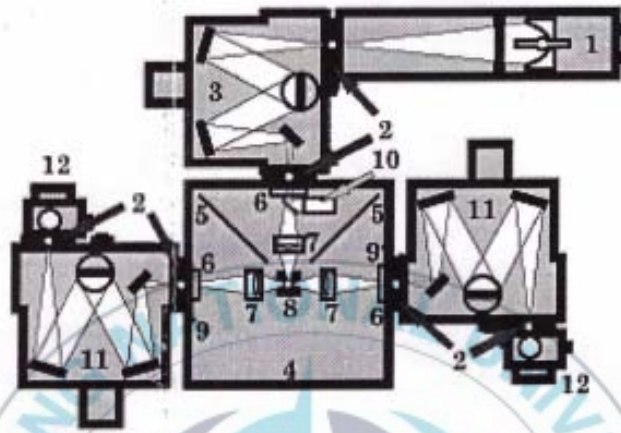
parameters were calculated using Powder-X diffraction analysis software

The morphology and size of samples were measured by means of field emission scanning electron microscope (FE-SEM, JEOL JSM-6700F). Both the photoluminescence and lifetime measurements of emission bands of the phosphors were recorded on a luminescence spectrophotometer (Photon Technology International (PTI)) with a Xe-arc lamp (60 W) as an excitation source. Schematic diagram and also a photograph of luminescence spectrophotometer (PTI) are shown in Fig. 3.3.





Figure 3.2 X-ray diffractometer (X'PERT PRO, PHILIPS).



1. Xe Arc Lamp (excitation source)	7. Excitation/emission optics
2. Adjustable slits	8. Cuvette holder
3. Excitation Monochromator	9. Excitation Correction
4. Sample compartment	10. Emission port shutter
5. Baffle	11. Emission Monochromator
6. Filter holders	12. PMT detectors

Figure 3.3 Schematic representation of the photoluminescence system.

IV. Results and discussions

4.1 Effect of the charge compensation of Eu^{3+} doped CaMoO_4 phosphors

Fig. 1 shows the XRD patterns of uncompensated $\text{Ca}_{0.95}\text{MoO}_4:0.05\text{Eu}^{3+}$ and compensated $\text{Ca}_{0.925}\text{MoO}_4:0.05\text{Eu}^{3+}$ phosphors sintered at 900°C for 5 h. All the diffraction peaks are well indexed to the tetragonal crystal from with the space group $I4_1/a$. And they matched well to the CaMoO_4 (JCPDS card no. 07-0212) without another impurity peaks, indicating that the Eu^{3+} ions are substituted into the Ca^{2+} sites of host lattice.

The crystallinity of compensated $\text{Ca}_{0.925}\text{MoO}_4:0.05\text{Eu}^{3+}$ phosphor is improved compared to the $\text{Ca}_{0.95}\text{MoO}_4:0.05\text{Eu}^{3+}$ phosphor, through the relatively high and sharp peaks in Fig. 4.1.1(a). The values of full width at half-maximum (FWHM) of the (1 1 2) crystal face are 0.12176 and 0.14074, corresponding to compensated and uncompensated, respectively. The value of FWHM of satisfied condition was decreased by a factor of 13.5%, thus it was showed higher crystallinity than charge unbalance.

As can be seen in Fig. 4.1.1(b), these main diffraction peaks were shifted towards to lower angles with charge compensation. It causes the change of the structural parameters due to charge unbalance. The structural parameters such as lattice constants, crystallite size and micro-strain of uncompensated $\text{Ca}_{0.95}\text{Eu}_{0.05}\text{MoO}_4$ and compensated $\text{Ca}_{0.925}\text{Eu}_{0.05}\text{MoO}_4$ were determined from the

XRD data in Table 4.1. The lattice constants were calculated using the following formula [43]:

$$\sin^2\theta = \frac{\lambda^2}{4} \left[\left\{ \frac{h^2+k^2}{a^2} \right\} + \left\{ \frac{l^2}{c^2} \right\} \right] \quad (1).$$

Where, θ is the diffraction angle, h , k and l are miller index of peak, and λ is X-ray wavelength (1.5406 Å). In Table 4.1, a value of $\text{Ca}_{0.925}\text{Eu}_{0.05}\text{MoO}_4$ increased than $\text{Ca}_{0.95}\text{Eu}_{0.05}\text{MoO}_4$, while c value nearly remains unchanged. That is, the lattice constant of compensated $\text{Ca}_{0.925}\text{MoO}_4:0.05\text{Eu}^{3+}$ phosphor is increased than uncompensated $\text{Ca}_{0.95}\text{MoO}_4:0.05\text{Eu}^{3+}$ phosphor.

The strain and crystallite size were estimated from the broadening of the diffraction peaks, and calculated using the Williamson and Hall relation [44].

$$\beta \cos\theta = \varepsilon(4\sin\theta) + \frac{\lambda}{D} \quad (2)$$

Where, β is the full width at half maximum (FWHM in radian), ε is the strain, and D is the grain size. The strain is calculated from the slope and the crystallite size is calculated from the intercept of a plot $\beta \cos\theta$ against $4\sin\theta$ in Fig. 4.1.2.

The strain can be observed negative value in table 4.1. The negative slope value indicates the compressive strain. Compressive strain is defined as deformation along a line segment that decreases in length when a load is applied [45]. The strain value of $\text{Ca}_{0.925}\text{Eu}_{0.05}\text{MoO}_4$ is increased than $\text{Ca}_{0.95}\text{Eu}_{0.05}\text{MoO}_4$, but it means that the influence on the strain was decreased. Therefore, the lattice constant is greatly increased along with a axis, and which can influence properties of the emission.

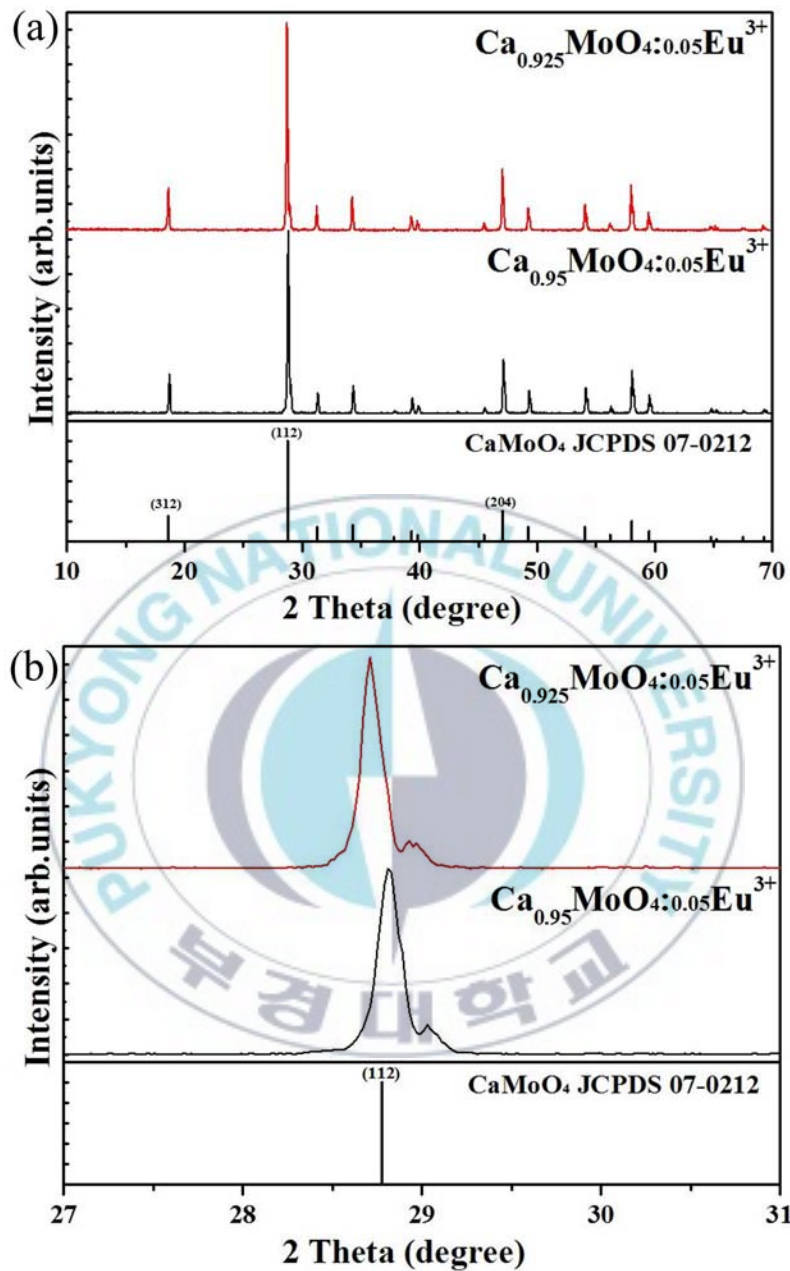


Figure 4.1.1 (a) XRD patterns of uncompensated $\text{Ca}_{0.95}\text{MoO}_4:0.05\text{Eu}^{3+}$ and compensated $\text{Ca}_{0.925}\text{MoO}_4:0.05\text{Eu}^{3+}$ phosphors and the reference data of JCPDS card No. 07-0212, (b) enlarged XRD near 27-30° (2θ) for (1 1 2) main peak.

Table 4.1 Structural parameters of satisfied the charge compensation condition and otherwise.

	Lattice constants (Å)		Cell volume (Å ³)	Crystallit e size (D) (nm)	Micro- stain (ε) (10 ⁻³)
	a=b	c			
JCPDS card	5.2429	11.373	312.17	-	-
Ca _{0.95} Eu _{0.05} MoO ₄	5.1622	11.4525	305.18	59.25	-12.23
Ca _{0.925} Eu _{0.05} MoO ₄	5.1847	11.4522	307.84	66.34	-7.35

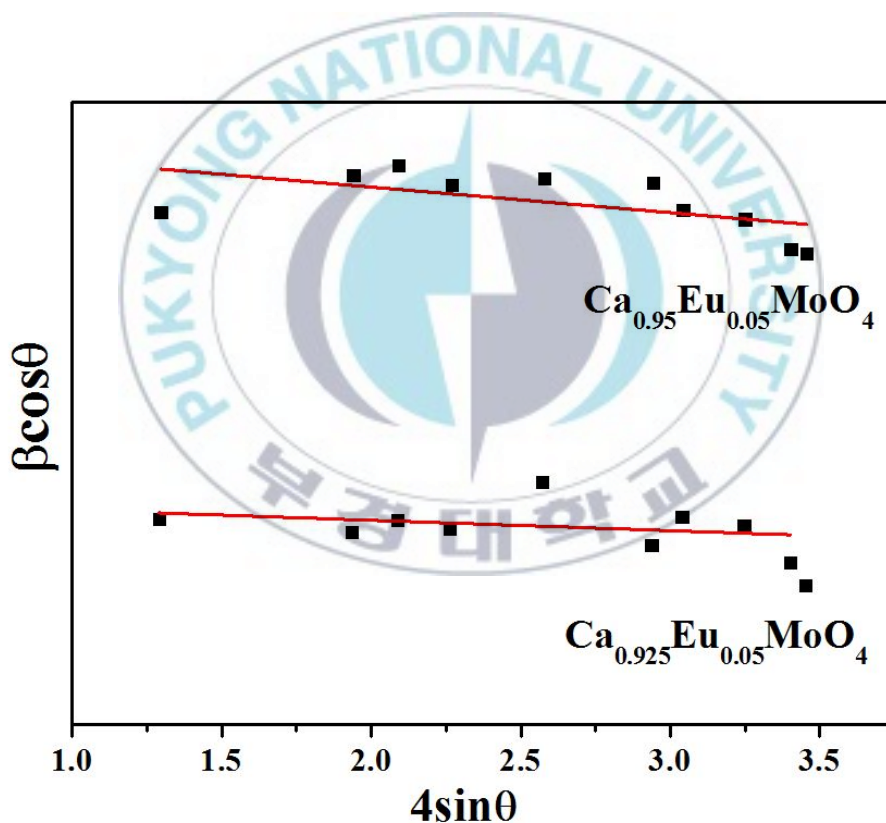


Figure 4.1.2 Plot of $\beta\cos\theta$ against $4\sin\theta$ for $\text{Ca}_{0.95}\text{MoO}_4:0.05\text{Eu}^{3+}$ and $\text{Ca}_{0.925}\text{MoO}_4:0.05\text{Eu}^{3+}$ phosphors.

The SEM images of the uncompensated $\text{Ca}_{0.95}\text{Eu}_{0.05}\text{MoO}_4$ and the compensated $\text{Ca}_{0.925}\text{Eu}_{0.05}\text{MoO}_4$ phosphors are shown in Fig. 4.1.3. Both the $\text{Ca}_{0.95}\text{Eu}_{0.05}\text{MoO}_4$ and $\text{Ca}_{0.925}\text{Eu}_{0.05}\text{MoO}_4$ images are confirmed that morphologies observed a spherical shape. When charge compensation is satisfied, the particle is increased the particle size, and has a smooth particle surface in Fig. 4.1.3 (c) and (b).

Fig. 4.1.4 shows the photoluminescence excitation (PLE) spectra of $\text{CaMoO}_4:\text{Eu}^{3+}$ phosphors by monitoring the emission wavelength at 617.5 nm. The excitation intensity of compensated $\text{Ca}_{0.925}\text{Eu}_{0.05}\text{MoO}_4$ is obviously higher than uncompensated $\text{Ca}_{0.95}\text{Eu}_{0.05}\text{MoO}_4$. The broad peak at 220-350 nm and sharp peak between 350-500 nm are observed. The broad peak is assigned to the contribution of charge transfer (CT) transition of $\text{O}^{2-} \rightarrow \text{Eu}^{3+}$ and $\text{O}^{2-} \rightarrow \text{Mo}^{6+}$ [46,47]. The $\text{O}^{2-} \rightarrow \text{Eu}^{3+}$ and $\text{O}^{2-} \rightarrow \text{Mo}^{6+}$ transition are attributed to the electron transitions from completely filled $2p$ orbital of the O^{2-} ion to partially filled $4f$ orbital of the Eu^{3+} or $5d$ orbital of Mo^{6+} . They are affected to the distance between the metal ion and the ligands [42,48].

The broad peak centered of $\text{Ca}_{0.95}\text{Eu}_{0.05}\text{MoO}_4$ (290.5 nm) is different from $\text{Ca}_{0.925}\text{Eu}_{0.05}\text{MoO}_4$ (302.5 nm) in showed Fig. 4.1.5. The broad bands have been fitted using two Gaussian function curves, and the results are in good agreement with the experimental data. The excitation spectrum of uncompensated $\text{Ca}_{0.95}\text{Eu}_{0.05}\text{MoO}_4$ has two wide bands centered at 278.5 nm and 298.5 nm, corresponding to CT band of the $\text{O}^{2-} - \text{Eu}^{3+}$ and $\text{O}^{2-} - \text{Mo}^{6+}$ interactions, respectively. The excitation spectrum of compensated $\text{Ca}_{0.925}\text{Eu}_{0.05}\text{MoO}_4$ has to

$O^{2-} - Eu^{3+}$ CT band at 288 nm and $O^{2-} - Mo^{6+}$ at 313 nm. Under the charge compensation condition is satisfied, CT band of $O^{2-} - Eu^{3+}$ and $O^{2-} - Mo^{6+}$ shifted towards the lower energy region due to the either particle size or covalent effect or both. In addition to this, improvement of crystallinity occurs. Unit cell volume increases with charge compensation due to decreasing defect. Thus, overall $O^{2-} - Eu^{3+}$ and $O^{2-} - Mo^{6+}$ bond distance per unit cell increases, and then it give enhance of covalent bond interaction. The enhancement of covalent bond interaction increases more CT process between O^{2-} to empty orbital of Eu^{3+}/Mo^{6+} . Increasing covalent bond interaction give the red shift in CT band of $O^{2-} - Eu^{3+}$ and $O^{2-} - Mo^{6+}$ [49].

The sharp excitation peaks due to intra-configurational $f-f$ transitions of Eu^{3+} ions are assigned to the electronic transitions of ${}^7F_0 \rightarrow {}^5D_4$, ${}^7F_0 \rightarrow {}^5L_7$, ${}^7F_0 \rightarrow {}^5L_6$, ${}^7F_0 \rightarrow {}^5D_3$ and ${}^7F_0 \rightarrow {}^5D_2$ at 365, 385, 397.5, 419 and 468 nm, respectively. The main excitation spectra are located at 397 nm, which matches the emission wavelength of near-UV GaN-based LEDs [3]. It means that this phosphor is suitable to be used for pc-white-LEDs based on InGaN LED chips.

The excitation intensity of $f-f$ transition on charge compensation is enhanced about 3.5 times than uncompensated $Ca_{0.95}MoO_4:0.05Eu^{3+}$. This is because crystallinity of phosphor is improved by the compensation effect, and crystal field of surrounding Eu^{3+} is distorted. The order of their compensation effect on the excitation intensity is consistent with crystallinity mentioned above.

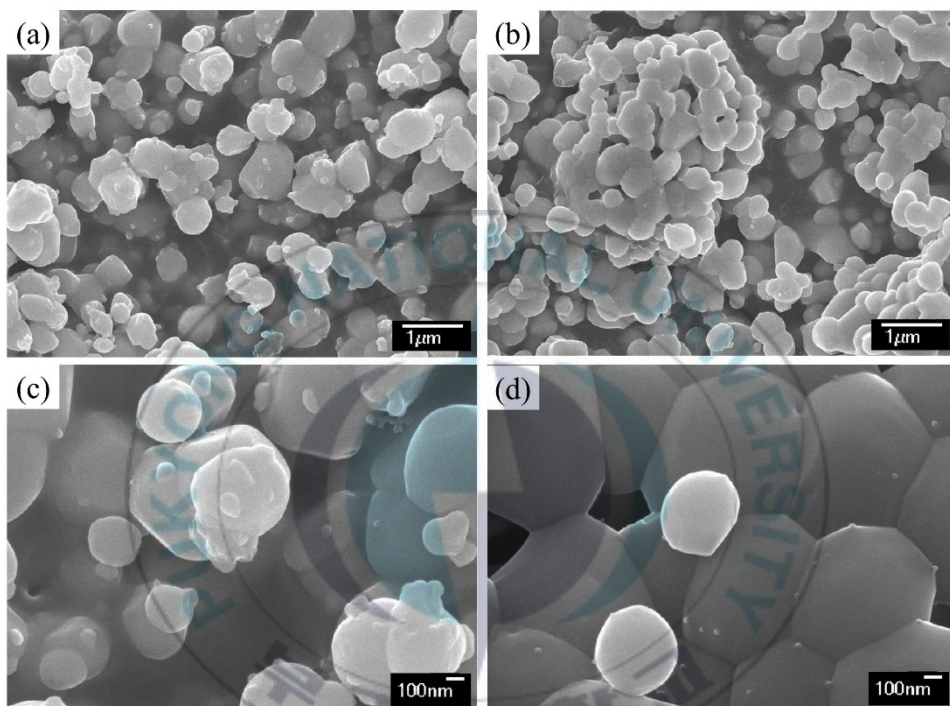


Figure 4.1.3 SEM image of (a, c) uncompensated $\text{Ca}_{0.95}\text{MoO}_4:0.05\text{Eu}^{3+}$ and (b, d) compensated $\text{Ca}_{0.925}\text{MoO}_4:0.05\text{Eu}^{3+}$.

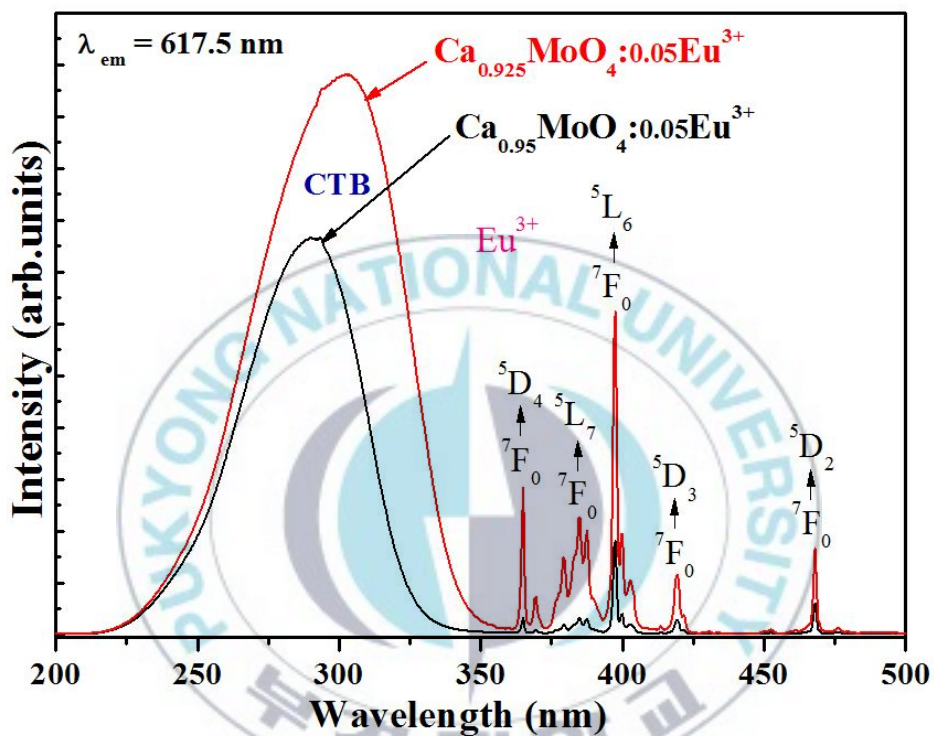


Figure 4.1.4 PLE spectra of uncompensated $\text{Ca}_{0.95}\text{MoO}_4:0.05\text{Eu}^{3+}$ and compensated $\text{Ca}_{0.925}\text{MoO}_4:0.05\text{Eu}^{3+}$ phosphors by monitoring the emission wavelength at 617.5 nm.

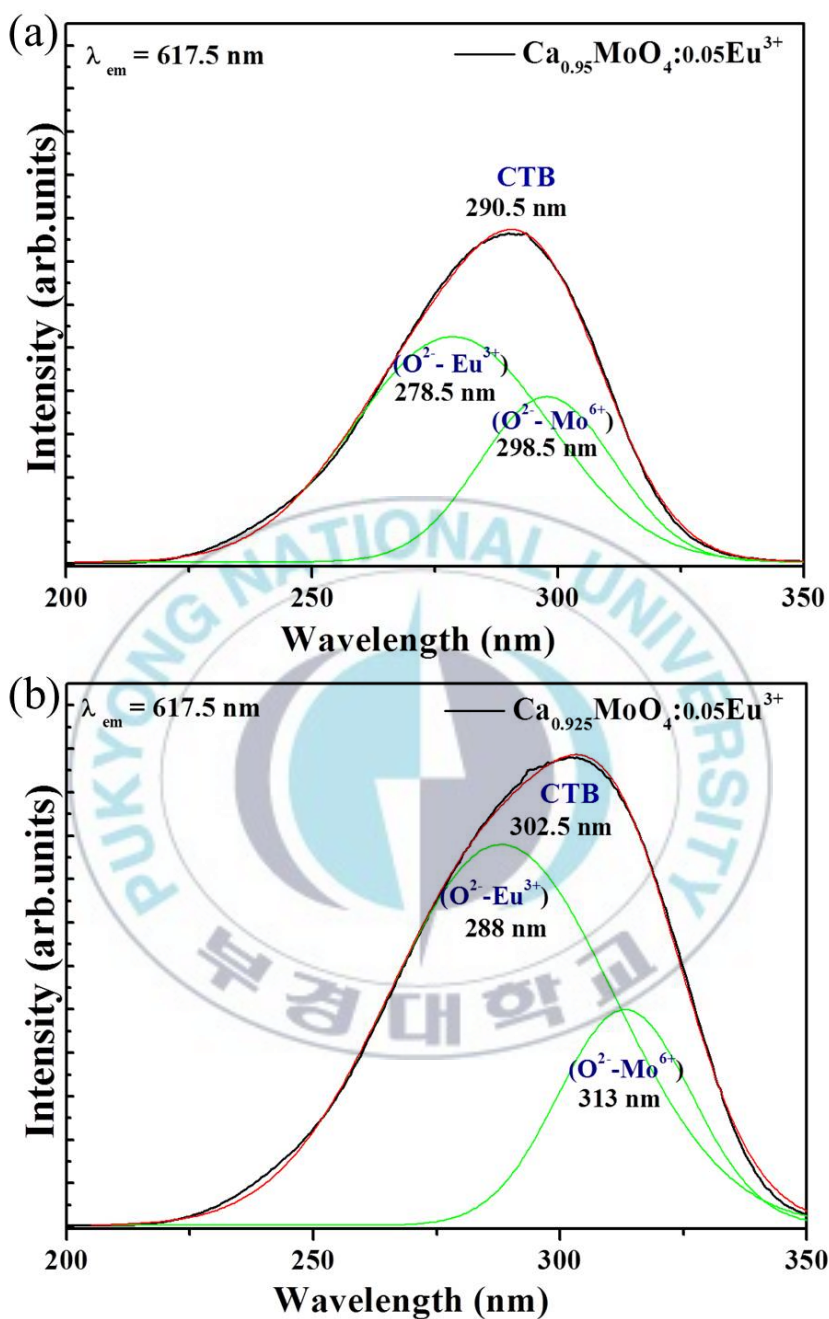


Figure 4.1.5 Gaussian fitting for PLE spectra of (a) uncompensated $\text{Ca}_{0.95}\text{MoO}_4:0.05\text{Eu}^{3+}$ and (b) compensated $\text{Ca}_{0.925}\text{MoO}_4:0.05\text{Eu}^{3+}$ phosphors.

Fig. 4.1.6 shows the PL spectra of uncompensated $\text{Ca}_{0.95}\text{Eu}_{0.05}\text{MoO}_4$ and compensated $\text{Ca}_{0.925}\text{Eu}_{0.05}\text{MoO}_4$ phosphors by exciting at 397.5 nm. The compensation condition approaches do not change the shape and position of PL spectra. However, there exists obvious difference among their emission intensity. The main emission is located at 617.5 nm from the Eu^{3+} electric dipole transition of ${}^5\text{D}_0 \rightarrow {}^7\text{F}_2$. On the other hand, other transitions from the ${}^5\text{D}_0$ excited state to ${}^7\text{F}_1$ ground states (such as the parity-allowed magnetic dipole transition of ${}^5\text{D}_0 \rightarrow {}^7\text{F}_1$ in 593.5 nm) are relatively weak. On the basis of the Judd-Ofelt theory [8], the electric dipole transition ${}^5\text{D}_0 \rightarrow {}^7\text{F}_2$ is hypersensitive of its local environment, and the emission intensity is strongly influenced by ligand ions in the crystals. But the magnetic dipole transition occurs regardless of environment. When ${}^5\text{D}_0 \rightarrow {}^7\text{F}_2$ transition appears dominantly, Eu^{3+} ion occupies the lattice site of non-centrosymmetric environment in the scheelite phases.

By careful analyzing the emission spectra, it is easy to notice that the emission intensity significantly increases about 3.7 times by charge compensation effect. Aumer et al. [50] reported that the lattice strain may be one of the reasons on the luminescence properties. The strain of uncompensated $\text{Ca}_{0.95}\text{Eu}_{0.05}\text{MoO}_4$ phosphor (-12.23%) is higher than compensated $\text{Ca}_{0.925}\text{Eu}_{0.05}\text{MoO}_4$ phosphor (-7.35%) and the luminescence intensity decreases with increasing compressive strain. This indicates that the non-radiative relaxation increases with increasing lattice strain [45]. In compensated $\text{Ca}_{0.925}\text{Eu}_{0.05}\text{MoO}_4$ phosphor, the decrement of mole number of Ca^{2+} relieves the charge unbalance to a certain extent. Therefore,

charge compensation suggests that both the crystallinity and emission intensity increases with decreasing strain.

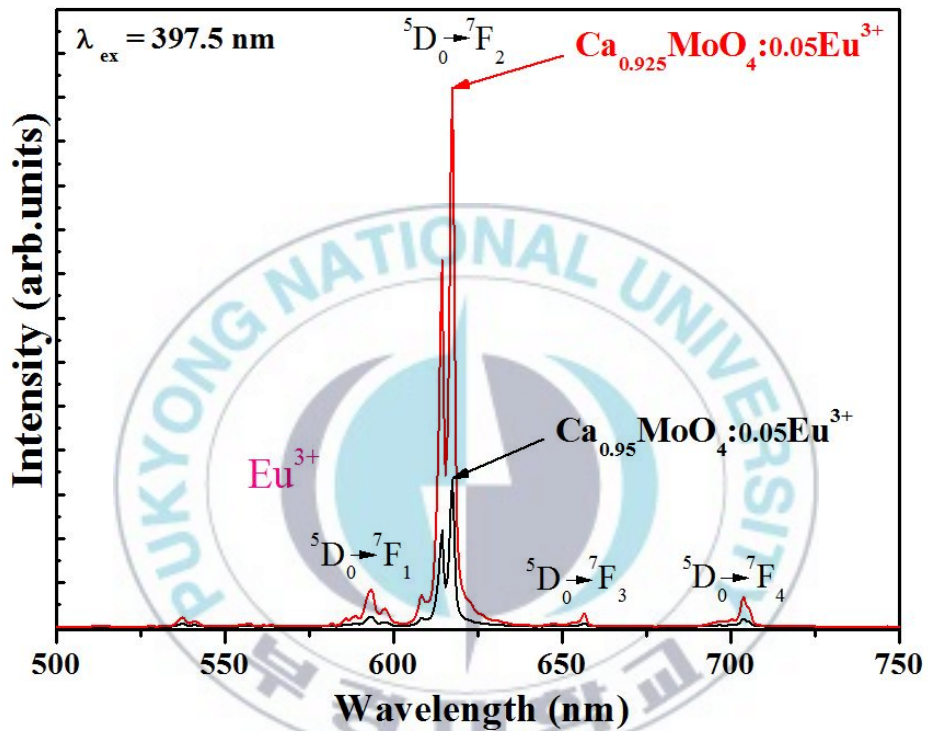


Figure 4.1.6 PL spectra of uncompensated $\text{Ca}_{0.95}\text{MoO}_4:0.05\text{Eu}^{3+}$ and compensated $\text{Ca}_{0.925}\text{MoO}_4:0.05\text{Eu}^{3+}$ phosphors under the excitation wavelength of 397.5 nm.

The decay curves for ${}^5D_0 \rightarrow {}^7F_2$ transition of the prepared phosphors under excitation at 397.5 nm were shown in Fig. 4.1.7. All the decay curves can be fitted well with a single exponential function given as $I(t) = A \exp(-t/\tau)$. The lifetime τ values for $\text{Ca}_{0.95}\text{Eu}_{0.05}\text{MoO}_4$ and $\text{Ca}_{0.925}\text{Eu}_{0.05}\text{MoO}_4$ are 0.428 and 0.476 ms, respectively. With the introducing charge compensation, the phosphor lifetime τ values increase. It should be noted that lifetime also abides by the changing rule of crystallinity, i.e. phosphor with better crystallinity has longer lifetime.



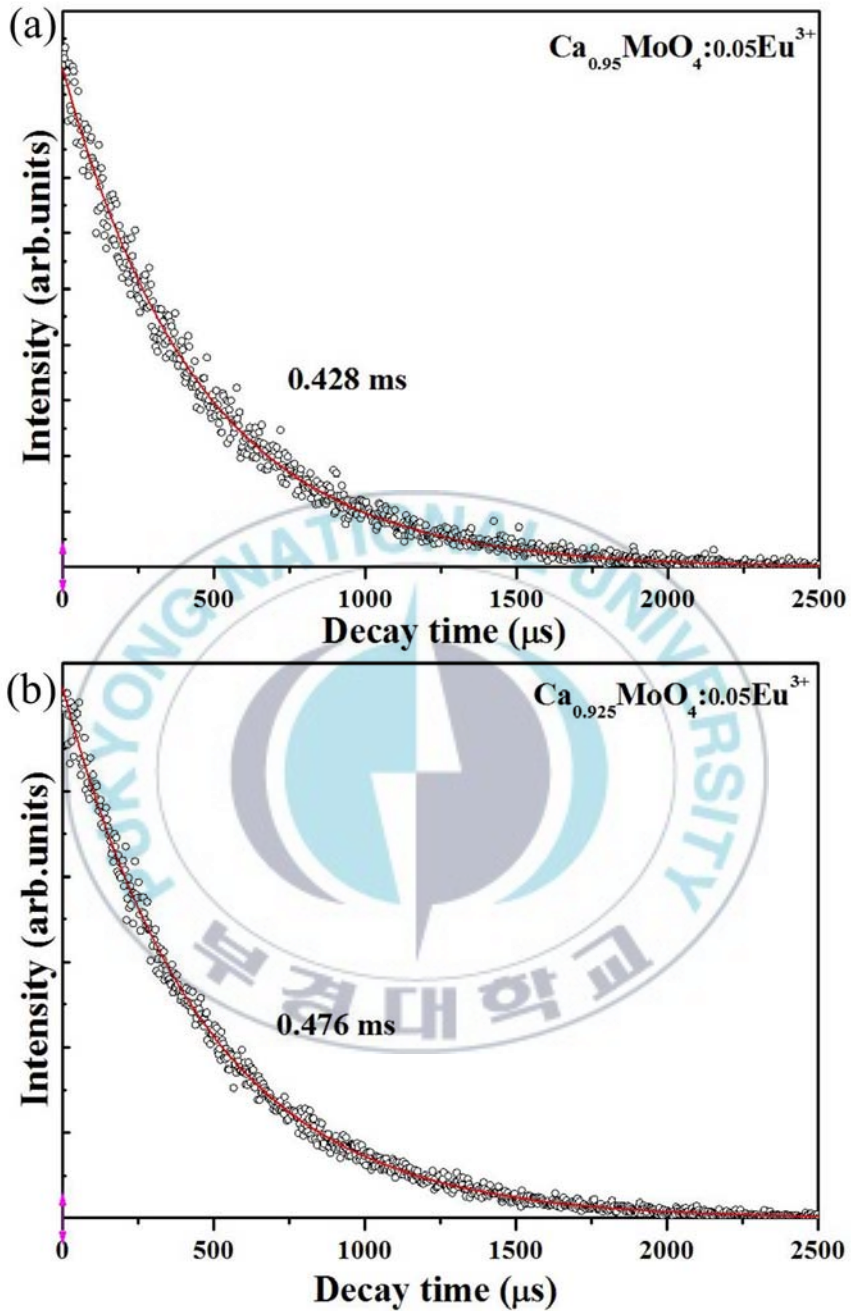


Figure 4.1.7 Decay curves of (a) uncompensated $\text{Ca}_{0.95}\text{MoO}_4:0.05\text{Eu}^{3+}$ and (b) compensated $\text{Ca}_{0.925}\text{MoO}_4:0.05\text{Eu}^{3+}$ phosphors as a function of charge compensation.

4.2 Luminescence properties of Eu^{3+} and Bi^{3+} co-doped

CaMoO_4 phosphors

Fig. 4.2.1 shows the XRD patterns of $\text{Ca}_{0.95-x}\text{MoO}_4:0.05\text{Eu}^{3+}, x\text{Bi}^{3+}$ phosphors co-doped with difference of Bi^{3+} ions sintered at 900°C for 5 h. As presented in this Fig. 4.2.1(a), the impurity peak of Bismuth oxide (Bi_2O_3) (*) was detected when the doping concentration of Bi^{3+} exceeds 0.02 mol. It is suggested that appropriate amount of 0.01 mol on Bi^{3+} doped in the lattice has no obvious influence to the crystal structure. Other peak are indexed to the tetragonal phase CaMoO_4 (JCPDS card no. 07-0212). CaMoO_4 belongs to the scheelite-like isostructure and the central Mo^{6+} metal ion is coordinated by four O^{2-} ions in tetrahedral symmetry (T_d).

Fig. 4.2.2 presents the PLE spectra of $\text{Ca}_{0.95-x}\text{MoO}_4:0.05\text{Eu}^{3+}, x\text{Bi}^{3+}$ phosphors co-doped with different concentrations of Bi^{3+} ions when emission was monitored at 617.5 nm. When Bi^{3+} ions are introduced in the phosphors, some changes in the wavelength range below 360 nm are observed. The broad band appears at the longer wavelength side of the CT band. In addition, the excitation spectra intensity at 324 nm form the $^1\text{S}_0 \rightarrow ^3\text{P}_1$ transition of Bi^{3+} ion enhanced with the increase of the Bi^{3+} doping ratio and reaches a maximum at 0.01 mol of Bi^{3+} . For samples with higher concentration of Bi^{3+} than 0.01 mol, the excitation intensity at 324 nm is weak to be observed, which shows there is a non-radiative energy transfer process among Bi^{3+} ions. The broad band in 0.01 mol of Bi^{3+} co-doped phosphor have been fitted using three Gaussian function

curves, and the results are in good agreement with the experimental data in Fig. 4.2.2 (b). The excitation spectrum has three wide bands centered at 246.5 nm, 290 nm and 327.5 nm, corresponding to charge transfer (CT) band of the $O^{2-} - Eu^{3+}$ and $O^{2-} - Mo^{6+}$ ions interactions [46,47,51] and the self-absorption of Bi^{3+} from ground state 1S_0 to the excited state 3P_1 , respectively [52,53].

While the sharp excitation peaks in the range of 360 – 500 nm are assigned to the intra-configurational $f-f$ transitions of Eu^{3+} ions in Fig. 4.2.2 (a). And the main excitation spectra are located at 397.5 nm corresponding to $^7F_0 \rightarrow ^5L_6$ transition of Eu^{3+} . The inset Fig. 4.2.2 (b) displays that the PLE intensity at 397.5 nm as a function of Bi^{3+} concentration. The both 397 and 468 nm excitation peak in 0.01 mol of Bi^{3+} are greatly enhanced about 2.6 – 4 times compared with undoped $Ca_{0.95}MoO_4:0.05Eu^{3+}$. While, above 0.01 mol of Bi^{3+} ion concentration, the intensity of $f-f$ transition are decreased gradually due to concentration quenching.

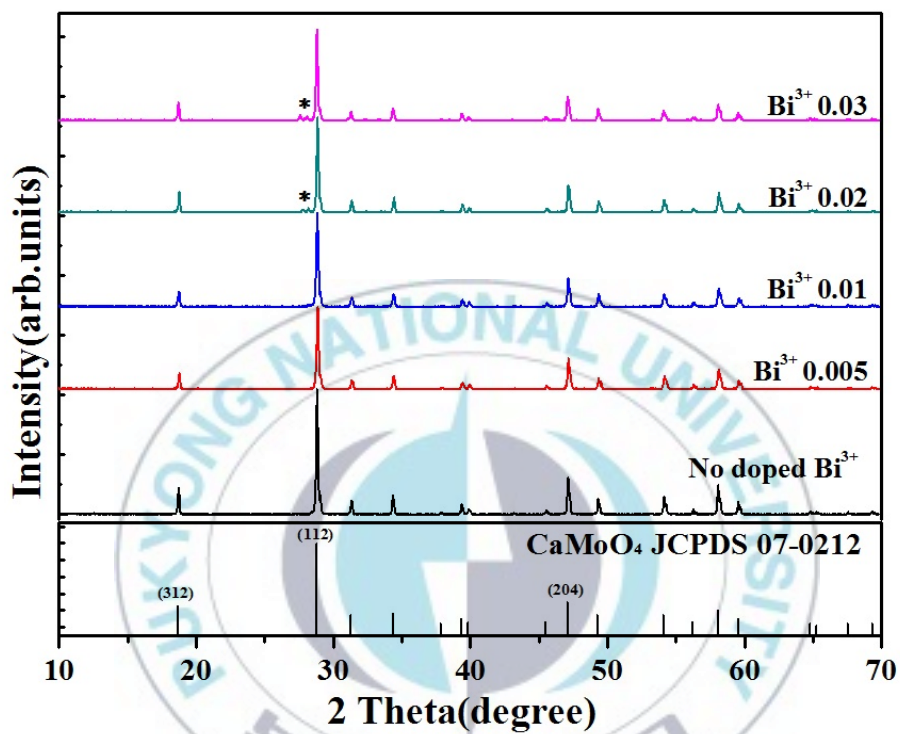


Figure 4.2.1 XRD patterns of $\text{Ca}_{0.95-x}\text{MoO}_4:0.05\text{Eu}^{3+}, x\text{Bi}^{3+}$ phosphors and the reference data of JCPDS card No. 07-0212.

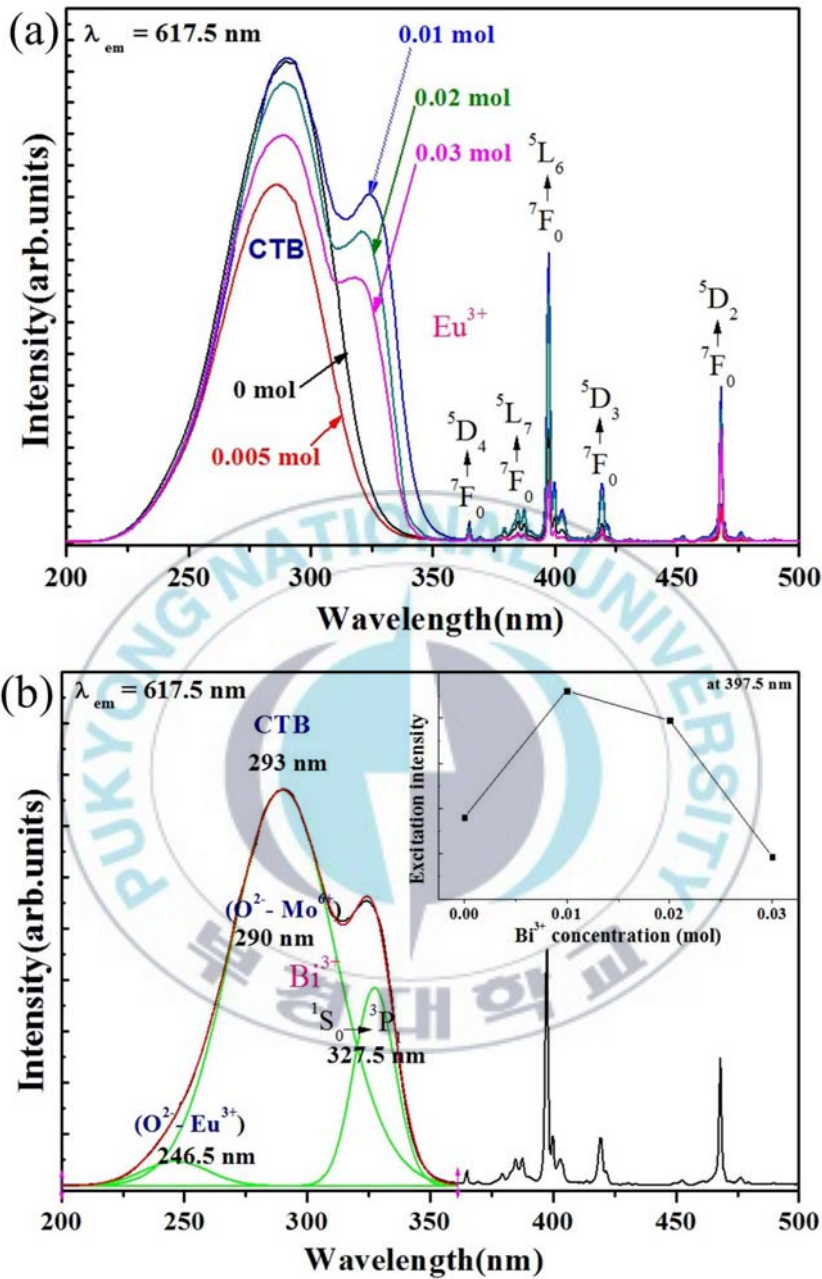


Figure 4.2.2 (a) PLE spectra of $\text{Ca}_{0.95-x}\text{MoO}_4:0.05\text{Eu}^{3+}, x\text{Bi}^{3+}$ phosphors by monitoring the emission wavelength at 617.5 nm and (b) Gaussian fitting for PLE spectra of $\text{Ca}_{0.94}\text{MoO}_4:0.05\text{Eu}^{3+}, 0.01\text{Bi}^{3+}$ phosphors. The inset represents the effect of Bi^{3+} concentration at 397.5 nm.

The emission spectra of $\text{Ca}_{0.95-x}\text{MoO}_4:0.05\text{Eu}^{3+}, x\text{Bi}^{3+}$ phosphors co-doped with different concentrations of Bi^{3+} under excitation at 327.5 nm is shown in Fig. 4.2.3. The emission spectrum belong to the characteristic emission Eu^{3+} ions corresponding to ${}^5\text{D}_0 \rightarrow {}^7\text{F}_J$ ($J = 0, 1, 2, 3, 4$) transitions. In order to improve the relative emission intensity of the $\text{Ca}_{0.95}\text{MoO}_4:0.05\text{Eu}^{3+}$ was partial co-doped with Bi^{3+} . The shapes and positions of emission spectra of $\text{Ca}_{0.95-x}\text{MoO}_4:0.05\text{Eu}^{3+}, x\text{Bi}^{3+}$ ($x = 0.005, 0.01, 0.02, 0.03$) do not change with the difference of Bi^{3+} concentration. However, the relative emission intensity changes evidently. The emission intensity of phosphor rapidly increases with increasing doped Bi^{3+} concentration up to 0.01 mol. When the concentration of Bi^{3+} ion is 0.01 mol, the emission intensity reaches its maximum, and then decreases for higher Bi^{3+} concentrations.

The emission peaks corresponding to Bi^{3+} are invisible in the Fig. 4.2.3 (a). But there are observed relatively low intensity from 400 to 500 nm in Fig. 4.2.3 (b). The emission of Bi^{3+} ions is hardly influenced with the absorption energy of Bi^{3+} owing to the energy transfer effect. The result shows that excitation energy by self-absorption of Bi^{3+} ion was transferred to Eu^{3+} levels nonradiation. Evidently from Fig. 4.2.2 (a), excitation intensity of Eu^{3+} ions increases with increasing Bi^{3+} concentration, which confirms that the efficient energy transfer occurs from the Bi^{3+} to the Eu^{3+} ion.

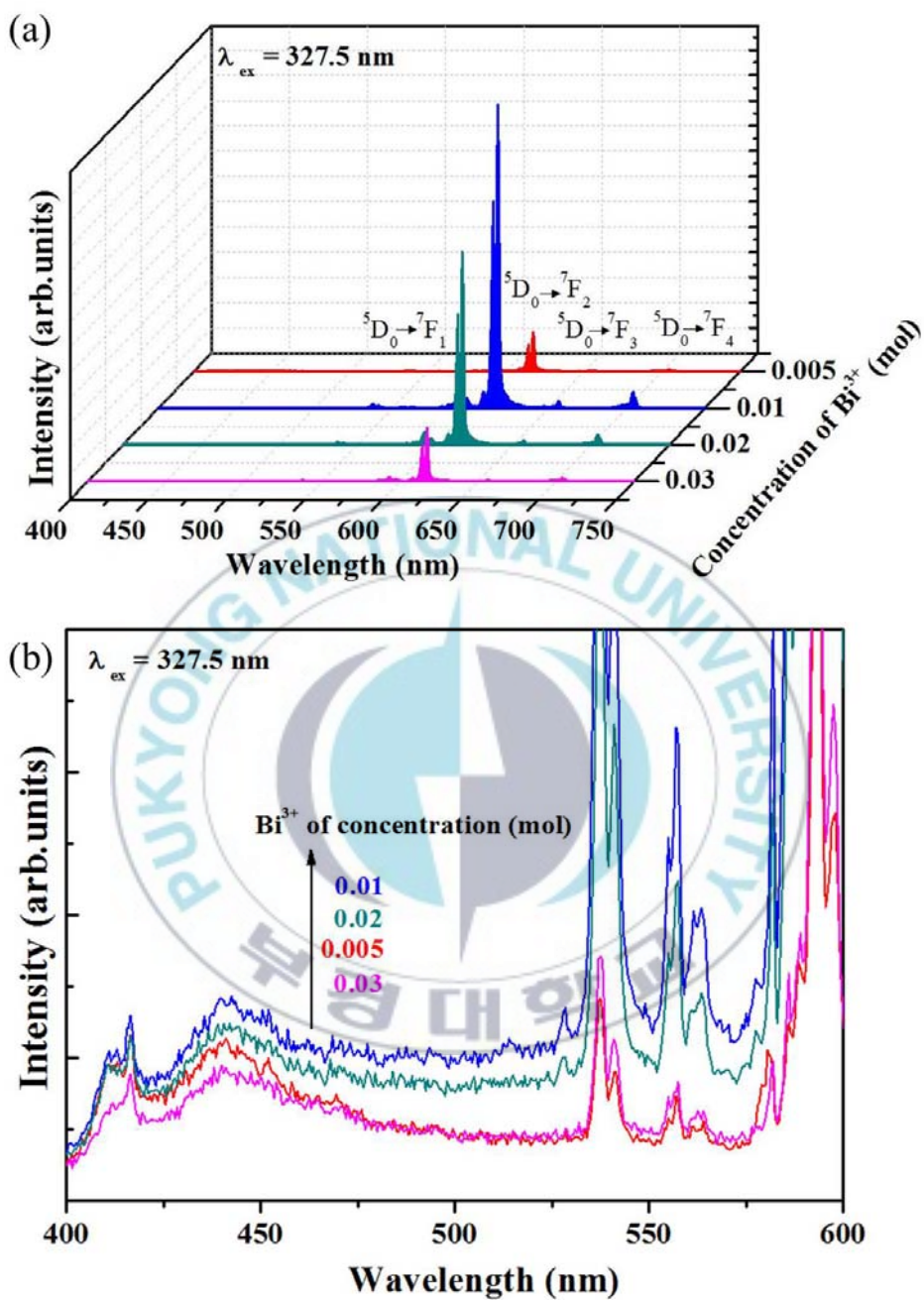


Figure (a) 4.2.3 PL spectra of $\text{Ca}_{0.95-x}\text{MoO}_4:0.05\text{Eu}^{3+}, x\text{Bi}^{3+}$ with different concentration of Bi^{3+} ion under the excitation wavelength of 327.5 nm and (b) enlarged PL spectra near 400-600 nm.

4.3 Effect of charge compensation on luminescence properties of Eu^{3+} and Bi^{3+} co-doping CaMoO_4 phosphors

Fig. 1 shows the XRD patterns of compensated $\text{Ca}_{0.925-1.5x}\text{MoO}_4:0.05\text{Eu}^{3+}$, $x\text{Bi}^{3+}$ phosphors doped with 0.05 mol of Eu^{3+} and difference concentration of Bi^{3+} ions. All of the diffraction peaks can be well indexed to the tetragonal phase CaMoO_4 (JCPDS card no. 07-0212), and there are no extra peaks from impurities of the variation of Bi^{3+} concentration in the patterns. It is suggested that appropriate amount of Bi^{3+} doped in the lattice has no obvious influence to the crystal structure. Eu^{3+} and Bi^{3+} are expected to occupy the Ca^{2+} site in this phosphor.

In this work, the phosphors are synthesized without and charge compensation ion, and structure obtained are still consistent with the scheelite phase with doped of Bi^{3+} . Therefore, we assume that the charge loss is compensated by Ca^{2+} vacancies (V_{Ca}) described by $3\text{Ca}^{2+} \rightarrow 2\text{Eu}^{3+} + V_{\text{Ca}}$ and $3\text{Ca}^{2+} \rightarrow 2\text{Bi}^{3+} + V_{\text{Ca}}$. Ionic radii mismatch among the Ca^{2+} , Eu^{3+} and Bi^{3+} are supposed to replace the Ca^{2+} vacancies and creation of other point defects in the host lattice.

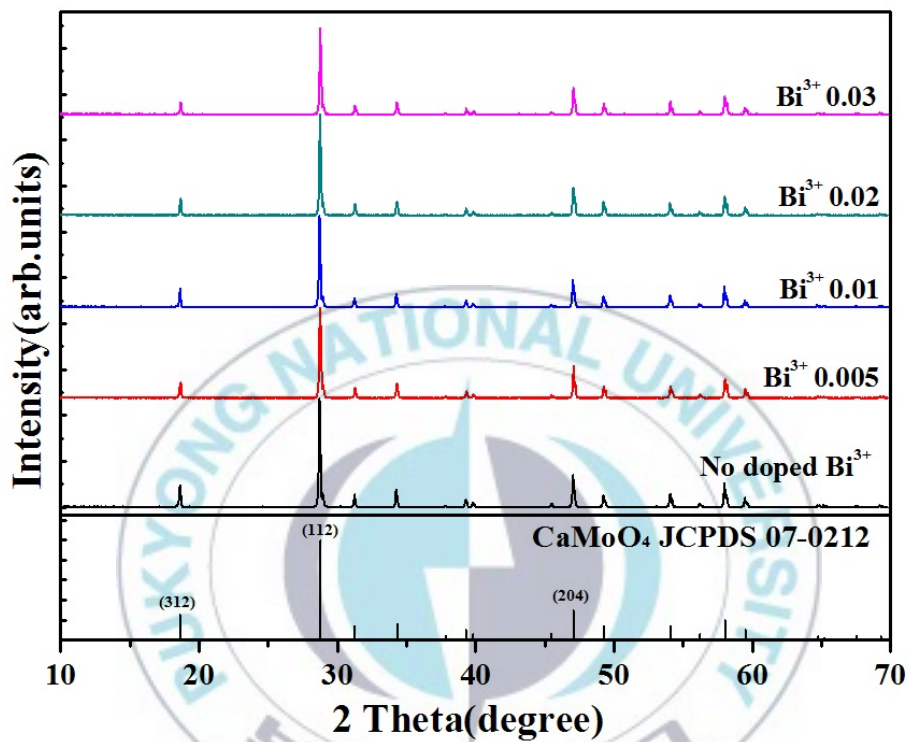


Figure 4.3.1 (a) XRD patterns of compensated $\text{Ca}_{0.925-1.5x}\text{MoO}_4:0.05\text{Eu}^{3+}, x\text{Bi}^{3+}$ phosphors and the reference data of JCPDS card No. 07-0212.

Fig. 4.3.2 presents the photoluminescence excitation (PLE) spectra of $\text{Ca}_{0.925-1.5x}\text{MoO}_4:0.05\text{Eu}^{3+}, x\text{Bi}^{3+}$ phosphors co-doped with different concentrations of Bi^{3+} ions when emission was monitored at 617.5 nm. When Bi^{3+} ions are incorporated into the $\text{Ca}_{0.925-1.5x}\text{Eu}_{0.05}\text{Bi}_x\text{MoO}_4$, broad band appears at 331 nm, which is attributed to the transition of $^6\text{S}_2 - 6s6p$ of Bi^{3+} ions. The excitation gets high intensity and further broadness from 220 to 370 nm upon the 0.01 mol of Bi^{3+} in the phosphor. The CT band is obvious that its intensity decreases gradually with the increasing Bi^{3+} concentration owing to the energy transfer from CT band to the transition of Bi^{3+} . The excitation intensity at 331 nm from the $^1\text{S}_0 \rightarrow ^3\text{P}_1$ transition of Bi^{3+} increases with increasing Bi^{3+} concentration until 0.01 mol. Above Bi^{3+} ion is 0.01 mol, the excitation peak at 331 nm is weak to be observed, which shows there is a non-radiative energy transfer process among Bi^{3+} ions.

Fig. 4.3.2 (b) shows the fitted spectrum of broad band on $\text{Ca}_{0.91}\text{MoO}_4:0.05\text{Eu}^{3+}, 0.01\text{Bi}^{3+}$ phosphor using three Gaussian function curves, and the results are in good agreement with the experimental data. The excitation spectrum has three wide bands centered at 280.5 nm, 297 nm, and 334.5 nm corresponding to charge transfer (CT) band of the O^{2-} to $\text{Eu}^{3+}/\text{Mo}^{6+}$ ions interactions [46,47,51] and the self-absorption of Bi^{3+} from $^1\text{S}_0$ to $^3\text{P}_1$, respectively [52,53].

While, the sharp excitation peaks from 360 to 500 nm are observed the typically $f - f$ transitions of Eu^{3+} ions in Fig. 4.3.2(a). And the strongest absorption peak in excitation spectra is located at 397 nm corresponding to

${}^7F_0 \rightarrow {}^5L_6$ transition of Eu^{3+} . The relative intensity at 397.5 nm is increased with the doping concentration of Bi^{3+} ions in the inset Fig. 4.3.2 (b). It reaches the maximum intensity at 0.01 mol, and then decreases. The 397 and 468 nm excitation peak in 0.01 mol of Bi^{3+} are greatly enhanced about 1.9 – 2.1 times compared with un-doped $\text{Ca}_{0.925}\text{MoO}_4:0.05\text{Eu}^{3+}$.

The emission spectra of $\text{Ca}_{0.925-1.5x}\text{MoO}_4:0.05\text{Eu}^{3+}, x\text{Bi}^{3+}$ phosphors co-doped with different concentrations of Bi^{3+} under excitation at 334.5 nm is shown in Fig. 4.3.3. All the emission peaks belong to the typical emission of Eu^{3+} ions. The emission of Bi^{3+} is hardly observed owing to the energy transfer from Bi^{3+} to Eu^{3+} ions. The doping concentrations of Bi^{3+} are changed to optimize the emission properties of Eu^{3+} . The dominant emission peak is the ${}^5D_0 \rightarrow {}^7F_2$ transition of Eu^{3+} at 617.5 nm, other transitions from the 5D_0 excited levels to 7F_J ($J = 1, 3, 4$) ground states are relatively weak. The emission intensity of Eu^{3+} are increases as the increasing dopant concentration of Bi^{3+} up to 0.01 mol and then decreases at higher concentrations. It can be seen that the optimal dopant concentration of Bi^{3+} is 0.01 mol.

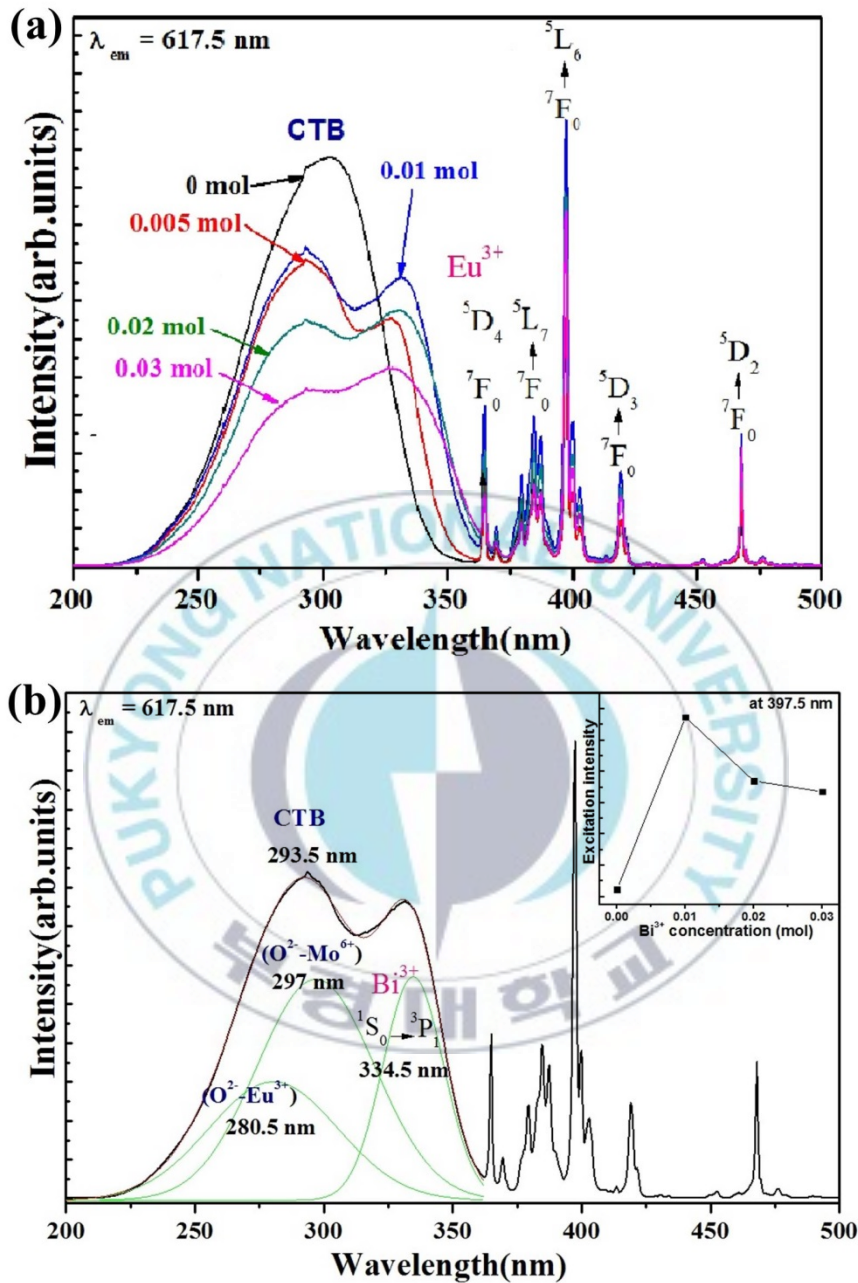


Figure 4.3.2 (a) PLE spectra of $\text{Ca}_{0.925-1.5x}\text{MoO}_4:0.05\text{Eu}^{3+}, x\text{Bi}^{3+}$ phosphors by monitoring the emission wavelength at 617.5 nm and (b) Gaussian fitting for PLE spectra of $\text{Ca}_{0.91}\text{MoO}_4:0.05\text{Eu}^{3+}, 0.01\text{Bi}^{3+}$ phosphors. The inset represents the effect of Bi^{3+} concentration at 397.5 nm.

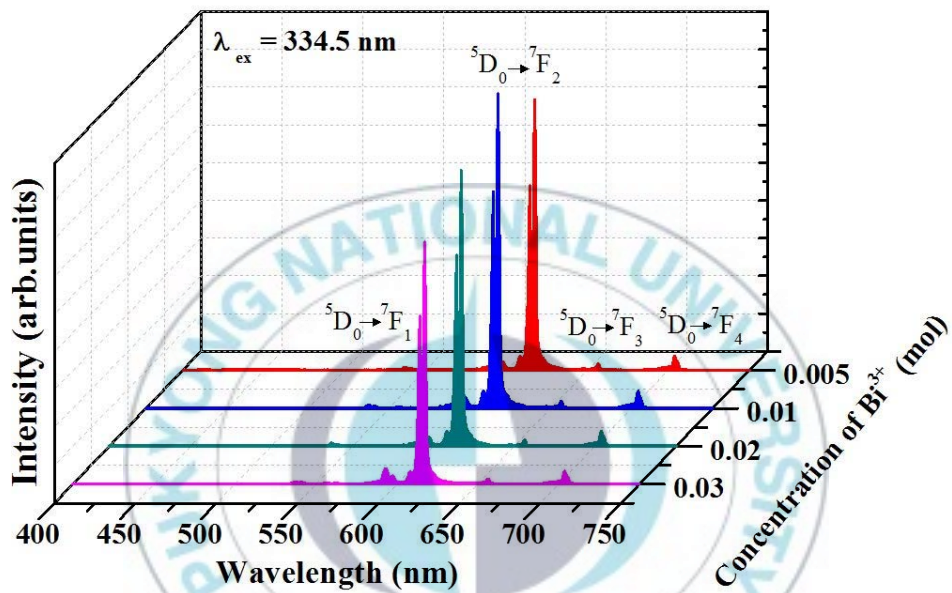


Figure 4.3.3 PL spectra of $\text{Ca}_{0.925-1.5x}\text{MoO}_4:0.05\text{Eu}^{3+}, x\text{Bi}^{3+}$ with different concentration of Bi^{3+} ion under the excitation wavelength of 334.5 nm.

When Bi^{3+} co-doped on the $\text{CaMoO}_4:\text{Eu}^{3+}$ phosphors, the crystallinity of compensated $\text{Ca}_{0.91}\text{Eu}_{0.05}\text{Bi}_{0.01}\text{MoO}_4$ phosphor is improved compared to the uncompensated $\text{Ca}_{0.94}\text{Eu}_{0.05}\text{Bi}_{0.01}\text{MoO}_4$ phosphor in Fig. 4.3.4(a). The values of full width at half-maximum (FWHM) of the (1 1 2) crystal face are 0.1572 and 0.1117, corresponding to compensated and uncompensated, respectively, and then the value of satisfied condition was decreased by a factor of 28.9 %. Also, Fig. 4.3.4(b) shows that main diffraction peaks were shifted towards lower angles with charge compensation. This indicates an expansion of the lattice cell according to the Bragg equation ($2d\sin\theta = \lambda$, where λ and θ are the wavelength of the X-ray and the diffraction angle, respectively). Therefore, the both crystallinity and the lattice constant of charge compensation condition is increased compared with uncompensated $\text{Ca}_{0.94}\text{Eu}_{0.05}\text{Bi}_{0.01}\text{MoO}_4$.

Fig. 4.3.5 shows PLE and PL spectra of uncompensated $\text{Ca}_{0.94}\text{MoO}_4:0.05\text{Eu}^{3+}$, 0.01Bi^{3+} and compensated $\text{Ca}_{0.91}\text{MoO}_4:0.05\text{Eu}^{3+}$, 0.01Bi^{3+} phosphors. With the compensated $\text{Ca}_{0.91}\text{Eu}_{0.05}\text{Bi}_{0.01}\text{MoO}_4$ phosphor, it occur the increasing intensity and red shift in the CTB. Also, self-absorption of Bi^{3+} shifted towards the lower energy region with charge compensation. The reason is that the crystal field splitting increases with charge compensation due to the enhancement of covalent bond interaction between O^{2-} to $\text{Eu}^{3+}/\text{Mo}^{6+}$. The excitation intensity of both the CTB as well as $f-f$ transition and the emission intensity are improved as doped of Bi^{3+} ions with charge compensation. The emission intensity is increased about 2.5 times compared with uncompensated $\text{Ca}_{0.94}\text{MoO}_4:0.05\text{Eu}^{3+}$, 0.01Bi^{3+} .

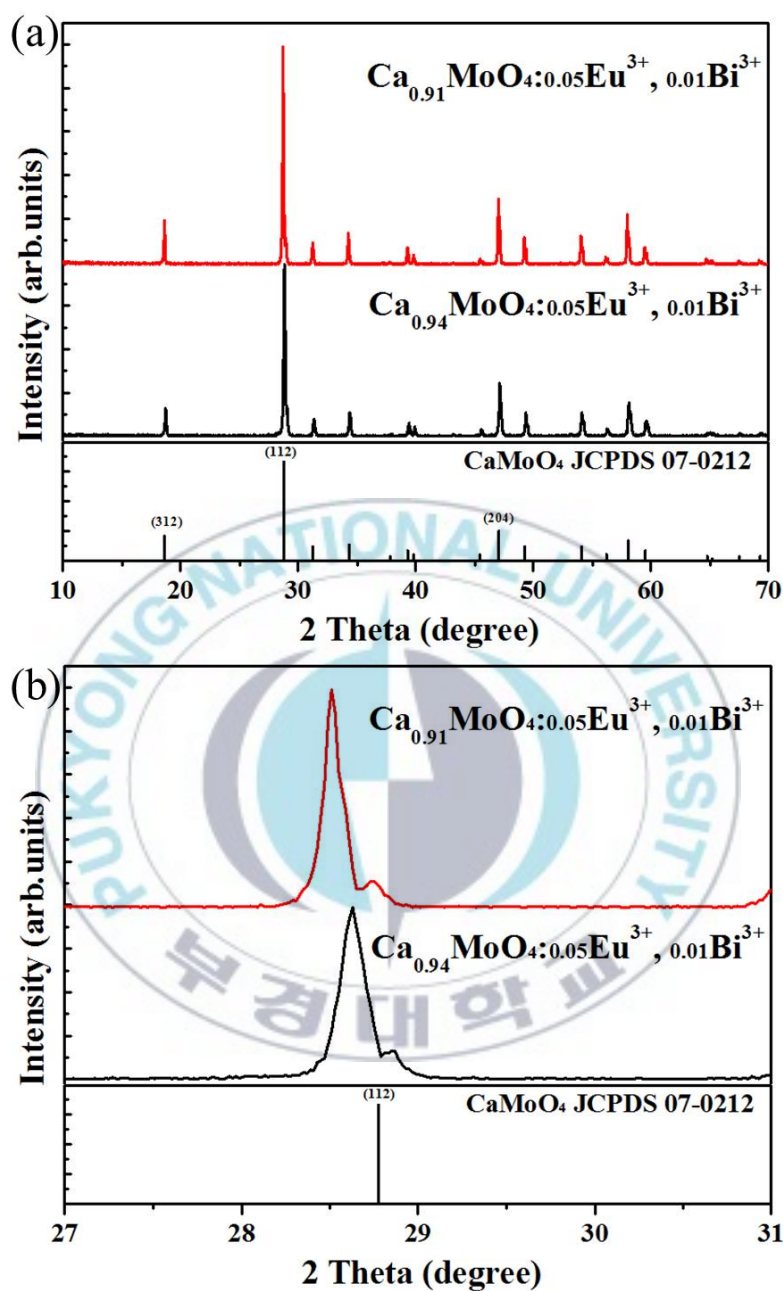


Figure 4.3.4 (a) XRD patterns of uncompensated $\text{Ca}_{0.94}\text{MoO}_4:0.05\text{Eu}^{3+}$, 0.01Bi^{3+} and compensated $\text{Ca}_{0.91}\text{MoO}_4:0.05\text{Eu}^{3+}$, 0.01Bi^{3+} phosphors, and the reference data of JCPDS card No. 07-0212, (b) enlarged XRD near 27-30° (2θ) for (1 1 2) main peak.

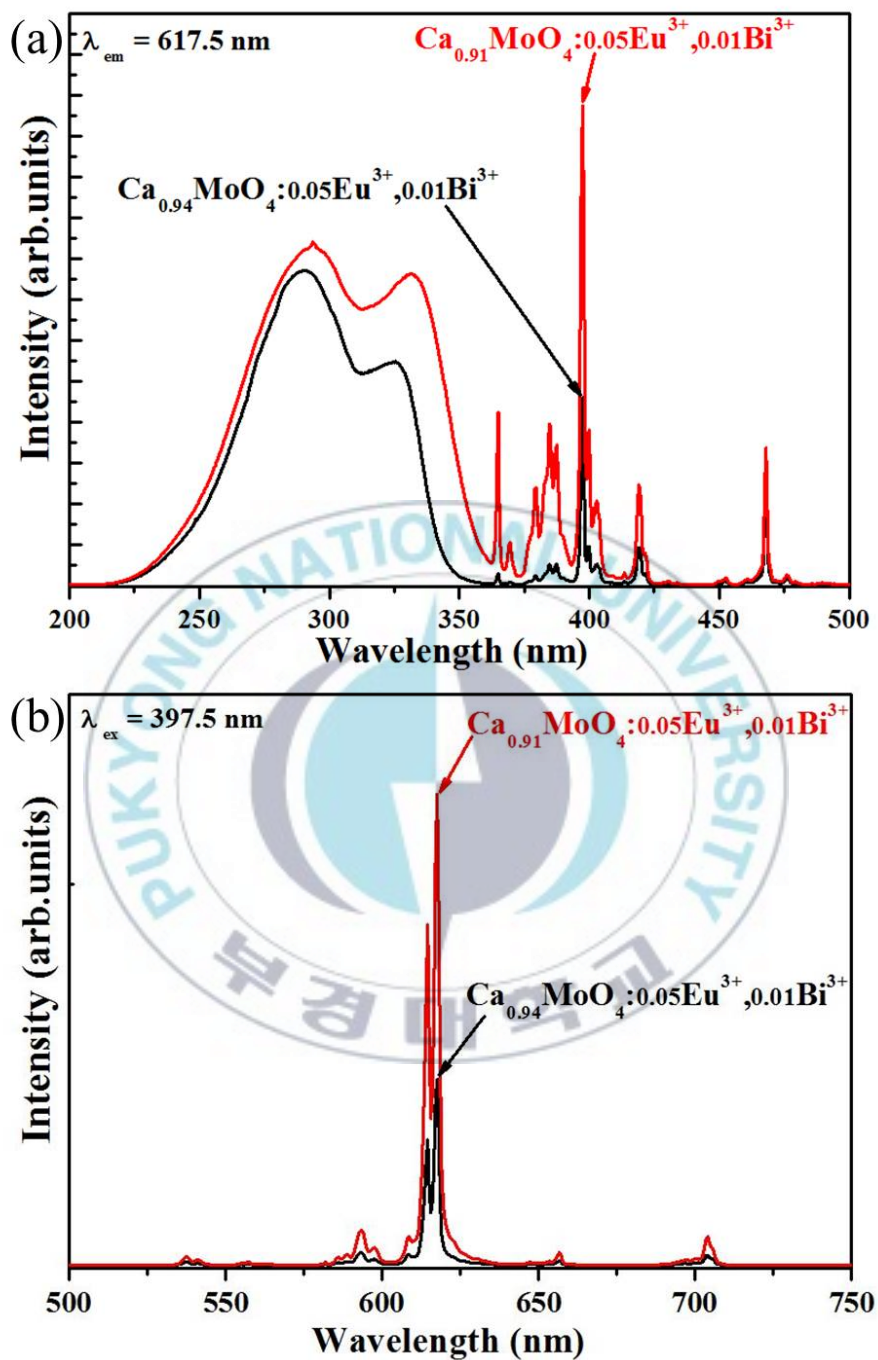


Figure 4.3.5 (a) PLE and (b) PL spectra of uncompensated $\text{Ca}_{0.94}\text{MoO}_4:0.05\text{Eu}^{3+}, 0.01\text{Bi}^{3+}$ and compensated $\text{Ca}_{0.91}\text{MoO}_4:0.05\text{Eu}^{3+}, 0.01\text{Bi}^{3+}$ phosphors.

In order to carefully analyze the emission spectra of all samples, it is easy to show compared with the emission intensity of the ${}^5D_0 \rightarrow {}^7F_2$ transition of Eu^{3+} . The Table 4.2 shows the comparison of emission intensities on $\text{Ca}_{0.95}\text{MoO}_4:0.05\text{Eu}^{3+}$, $\text{Ca}_{0.925}\text{MoO}_4:0.05\text{Eu}^{3+}$, $\text{Ca}_{0.94}\text{MoO}_4:0.05\text{Eu}^{3+}$, 0.01Bi^{3+} and $\text{Ca}_{0.91}\text{MoO}_4:0.05\text{Eu}^{3+}$, 0.01Bi^{3+} under excitation wavelength of 397.5 nm. The emission intensity of compensated $\text{Ca}_{0.925}\text{MoO}_4:0.05\text{Eu}^{3+}$ is improved 3.67 times than uncompensated $\text{Ca}_{0.95}\text{MoO}_4:0.05\text{Eu}^{3+}$. And then, the emission intensity of $\text{Ca}_{0.91}\text{MoO}_4:0.05\text{Eu}^{3+}$, 0.01Bi^{3+} is 6.2 times stronger than uncompensated $\text{Ca}_{0.95}\text{MoO}_4:0.05\text{Eu}^{3+}$ with un-doped Bi^{3+} . The result indicates that appropriate luminescence efficiency is related not only charge compensation but also addition of Bi^{3+} . Of all synthesized phosphors, $\text{Ca}_{0.91}\text{MoO}_4:0.05\text{Eu}^{3+}$, 0.01Bi^{3+} phosphor exhibit the strongest red emission.

Fig. 4.3.6 shows the PL spectra of composition-optimized $\text{Ca}_{0.91}\text{MoO}_4:0.05\text{Eu}^{3+}$, 0.01Bi^{3+} phosphor and commercial red phosphor $\text{Y}_2\text{O}_3:\text{Eu}^{3+}$ under excitation wavelength of 397.5 nm. The main emission peak at 613 nm of $\text{Y}_2\text{O}_3:\text{Eu}^{3+}$ phosphor is ascribed to Eu^{3+} transition of ${}^5D_0 \rightarrow {}^7F_2$. The integral emission intensity of $\text{Ca}_{0.91}\text{MoO}_4:0.05\text{Eu}^{3+}$, 0.01Bi^{3+} phosphor is 3.4 times higher than $\text{Y}_2\text{O}_3:\text{Eu}^{3+}$ phosphor, indicating that $\text{Ca}_{0.91}\text{MoO}_4:0.05\text{Eu}^{3+}$, 0.01Bi^{3+} phosphor is a promising red phosphor for white-light LEDs.

Table 4.2 The ${}^5D_0 \rightarrow {}^7F_2$ relative intensity of phosphors. (The intensity of $\text{Ca}_{0.95}\text{Eu}_{0.05}\text{MoO}_4$ is regarded as 1.00.)

Phosphors	Excitation wavelength (nm)	${}^5D_0 \rightarrow {}^7F_2$ relative intensity
$\text{Ca}_{0.95}\text{MoO}_4:0.05\text{Eu}^{3+}$	397.5	1.00
$\text{Ca}_{0.925}\text{MoO}_4:0.05\text{Eu}^{3+}$	397.5	3.67
$\text{Ca}_{0.94}\text{MoO}_4:0.05\text{Eu}^{3+}, 0.01\text{Bi}^{3+}$	397.5	2.45
$\text{Ca}_{0.91}\text{MoO}_4:0.05\text{Eu}^{3+}, 0.01\text{Bi}^{3+}$	397.5	6.20
$\text{Y}_2\text{O}_3\text{Eu}^{3+}$	397.5	2.32

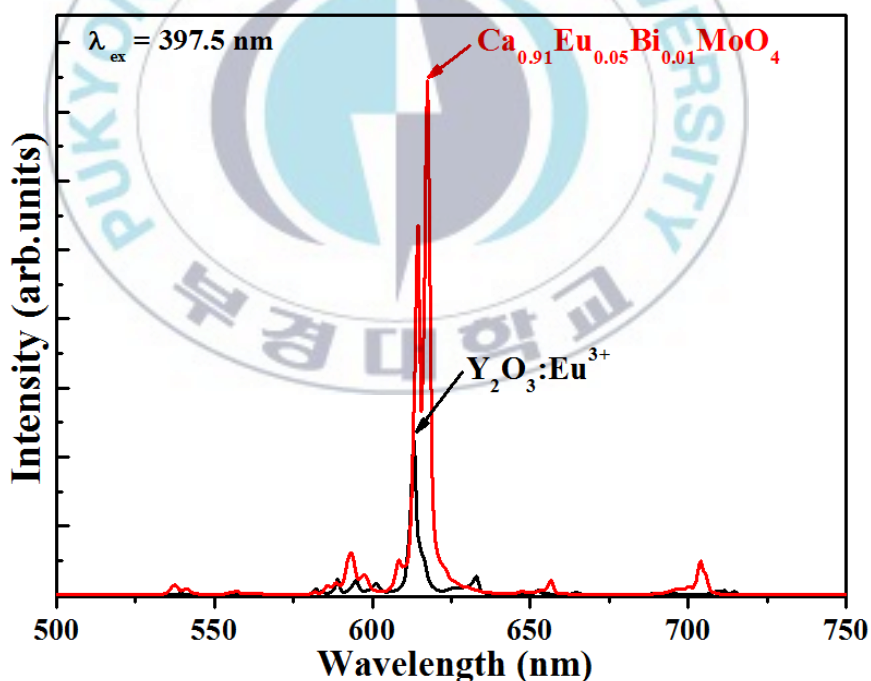


Figure 4.3.6 PL spectra of commercial $\text{Y}_2\text{O}_3:\text{Eu}^{3+}$ and compensated $\text{Ca}_{0.91}\text{Eu}_{0.05}\text{Bi}_{0.01}\text{MoO}_4$ phosphors monitoring excitation wavelength at 397.5 nm.

V. Conclusions

In this work, synthesis and luminescence properties of Eu^{3+} and Bi^{3+} co-doped in CaMoO_4 phosphors related to the charge compensation have been investigated in detail. The phosphors studied in this work were prepared using high energy ball milling.

When charge compensation condition ($\text{Ca}_{0.925}\text{MoO}_4:0.05\text{Eu}^{3+}$) is satisfied, the crystallinity is improved, and the lattice constant is increased than uncompensated $\text{Ca}_{0.95}\text{MoO}_4:0.05\text{Eu}^{3+}$ phosphors. In addition, CT band of $\text{Eu}^{3+} - \text{O}^{2-}$ and $\text{Mo}^{6+} - \text{O}^{2-}$ shifted towards the lower energy region by charge compensators. This is due to the increased covalent bond interaction between the $\text{Eu}^{3+}/\text{Mo}^{6+}$ and O^{2-} ions. The main emission peak of compensated $\text{Ca}_{0.925}\text{MoO}_4:0.05\text{Eu}^{3+}$ is located at 617.5 nm, and the relative emission intensity enhances about 3.7 times than that of $\text{Ca}_{0.95}\text{MoO}_4:0.05\text{Eu}^{3+}$.

Appropriate amount of Bi^{3+} ion is introduced into $\text{Ca}_{0.95}\text{MoO}_4:0.05\text{Eu}^{3+}$, the intensities of both excitation and emission are evidently improved. Also, the self-absorption of Bi^{3+} is observed in excitation spectra. The self-absorption of Bi^{3+} from ground state $^1\text{S}_0$ to the excited state $^3\text{P}_1$ is located at 327.5 nm. The excitation intensity of the sample including 0.01 mol of Bi^{3+} is increased about 2.6 – 4 times compared with un-doped $\text{Ca}_{0.95}\text{MoO}_4:0.05\text{Eu}^{3+}$. The emission spectra excited self-absorption of Bi^{3+} are hardly observed the emission peak of Bi^{3+} ion, whereas emission peak of Eu^{3+} ion is increased. It was clearly suggested which the energy transfer from Bi^{3+} to Eu^{3+} . The intensity of the emission and

excitation spectra increases with the increase of Bi^{3+} concentration. The optimum concentration for the luminescence of Bi^{3+} in $\text{CaMoO}_4:\text{Eu}^{3+}$ is about 0.01 mol.

When the charge compensation conditions are satisfied, the PL emission of Bi^{3+} co-doped in $\text{CaMoO}_4:\text{Eu}^{3+}$ phosphors have been observed maximum intensity at the Bi^{3+} concentration of 0.01 mol. The diffraction peaks are no impurities peaks of the variation of Bi^{3+} concentration. The excitation peak of self-absorption on Bi^{3+} is located at 331 nm, and excitation main peak is 397.5 nm corresponding to Eu^{3+} transition of ${}^7\text{F}_0 \rightarrow {}^5\text{L}_6$. The dominant peak is the ${}^5\text{D}_0 \rightarrow {}^7\text{F}_2$ transition at 617.5 nm, emission intensity enhanced as the increasing concentration of Bi^{3+} up to 0.01 mol, and then decreases at higher concentrations. It is attributed energy transfer from Bi^{3+} to Eu^{3+} .

In addition, with the compensated $\text{Ca}_{0.91}\text{MoO}_4:0.05\text{Eu}^{3+}, 0.01\text{Bi}^{3+}$ phosphor, it occur the increasing intensity of excitation and emission compared with uncompensated $\text{Ca}_{0.94}\text{MoO}_4:0.05\text{Eu}^{3+}, 0.01\text{Bi}^{3+}$. The self-absorption of Bi^{3+} of $\text{Ca}_{0.91}\text{MoO}_4:0.05\text{Eu}^{3+}, 0.01\text{Bi}^{3+}$ shifted towards the lower energy region owing to the crystal field splitting. Also, emission intensity is increased about 2.5 times than uncompensated $\text{Ca}_{0.94}\text{MoO}_4:0.05\text{Eu}^{3+}, 0.01\text{Bi}^{3+}$. The result indicates that appropriate dopant of Bi^{3+} ions is related with charge compensation.

Of these materials, $\text{Ca}_{0.91}\text{MoO}_4:0.05\text{Eu}^{3+}, 0.01\text{Bi}^{3+}$ exhibits the strongest red emission. Upon excitation wavelength of 397.5 nm, the main emission peak of $\text{Y}_2\text{O}_3:\text{Eu}^{3+}$ is located at 613 nm, whereas $\text{Ca}_{0.91}\text{MoO}_4:0.05\text{Eu}^{3+}, 0.01\text{Bi}^{3+}$ is 617.5 nm. The integral emission intensity of $\text{Ca}_{0.91}\text{MoO}_4:0.05\text{Eu}^{3+}, 0.01\text{Bi}^{3+}$ phosphor under excitation wavelength of 397.5 nm is about 3.4 times higher than that of

commercial $\text{Y}_2\text{O}_3:\text{Eu}^{3+}$ phosphor.



References

- [1] M. Zhang, Y. Liang, W. Huang, Z. Xia, D. Yu, Y. Lan, G. Li and W. Zhou, *Mater. Res. Bull.* **57** (2014) 231.
- [2] S. Ye, F. Xiao, Y. X. Pan, Y. Y. Ma and Q. Y. Zhang, *Materials Science and Engineering: R* **71** (2010) 1.
- [3] C. C. Lin, R. Liu, C. C. Lin and R. Liu, *J. Phys. Chem. Lett.* **2** (2011) 1268.
- [4] H. Höpfe A., *Angew. Chem. Int. Ed.* **48** (2009) 3572.
- [5] C. Feldmann, T. Justel, C. R. Ronda and P. J. Schmidt, *Adv. Funct. Mater.* **13** (2003) 511.
- [6] Y. Chang, C. Liang, S. Yan and Y. Chang, *J. Phys. Chem.C* **114** (2010) 3645.
- [7] L. Chen, K. Chen, C. C. Lin, C. Chu, S. Hu, M. Lee and R. S. Liu, *J. Comb. Chem.* **12** (2010) 587.
- [8] W. M. Yen, S. Shionoya and H. Yamamoto, "Phosphor handbook" CRC Press, (1999).
- [9] C. R. Ronda, *J. Lumin* **72–74** (1997) 49.
- [10] T. Chengaiah, C. K. Jayasankar, K. Pavani, T. Sasikala and L. R. Moorthy, *Opt. Commun.* **312** (2014) 233.

- [11] X. Li, L. Guan, M. Sun, H. Liu, Z. Yang, Q. Guo and G. Fu, *J. Lumin* **131** (2011) 1022.
- [12] Z. Yang, C. Hou, G. Duan, F. Yang, P. Liu, C. Wang, L. Liu and G. Dong, *J. Alloy. Compd.* **604** (2014) 346.
- [13] J. Liu, H. Lian and C. Shi, *Opt. Mater.* **29** (2007) 1591.
- [14] Y. Hu, W. Zhuang, H. Ye, D. Wang, S. Zhang and X. Huang, *J. Alloy. Compd.* **390** (2005) 226.
- [15] E. Cavalli, F. Angiuli, A. Belletti and P. Boutinaud, *Opt. Mater.* **36** (2014) 1642.
- [16] A. Xie, X. Yuan, Y. Shi, F. Wang and J. Wang, *J. Am. Ceram. Soc.* **92** (2009) 2254.
- [17] S. Neeraj, N. Kijima and A. K. Cheetham, *Chem. Phys. Lett.* **387** (2004) 2.
- [18] L. Wan, S. Lü, L. Sun and X. Qu, *Opt. Mater.* **36** (2014) 628.
- [19] S. Yan, J. Zhang, X. Zhang, S. Lu, X. Ren, Z. Nie and X. Wang, *J. Phys. Chem. C* **111** (2007) 13256.
- [20] P. Boutinaud, *Inorg. Chem.* **52** (2013) 6028.
- [21] H. Zhu, Z. Xia, H. Liu, R. Mi and Z. Hui, *Mater. Res. Bull.* **48** (2013) 3513.

- [22] G. Blasse and B. C. Grabmarier, "Luminescent materials" Springer Berlin Heidelberg, , Springer-Verlag Berlin Heidelberg, (1994).
- [23] V. B. Bhatkar, "Luminescence study of silicate and vanadate based phosphors: Luminescence, silicates, vanadates" LAP LAMBERT Academic Publishing, (2012).
- [24] C. R. Ronda, "Luminescence: From theory to applications" Wiley-VCH Verlag GmbH & Co. KGaA, Weinheim, (2008).
- [25] G. H. Dieke, H. M. Crosswhite and H. Crosswhite, "Spectra and energy levels of rare earth ions in crystals" Interscience, New York, (1968).
- [26] J. Singh, "Optical properties of condensed matter and applications" John Wiley & Sons, (2006).
- [27] W. Carnall, G. Goodman, K. Rajnak and R. Rana, *J. Chem. Phys.* **90** (1989) 3443.
- [28] R. t. Shannon, *Acta Crystallog. A* **32** (1976) 751.
- [29] C. Guo, F. Gao, Y. Xu, L. Liang, F. G. Shi and B. Yan, *J. Phys. D* **42** (2009) 095407.
- [30] W. A. I. Tabaza, H. C. Swart and R. E. Kroon, *J. Lumin* **148** (2014) 192.
- [31] A. A. Setlur and A. M. Srivastava, *Opt. Mater.* **29** (2006) 410.

- [32] H. Fukada, M. Konagai, K. Ueda, T. Miyata and T. Minami, *Thin Solid Films* **517** (2009) 6054.
- [33] J. H. Chung, J. H. Ryu, J. W. Eun, J. H. Lee, S. Y. Lee, T. H. Heo, B. G. Choi and K. B. Shim, *J. Alloy. Compd.* **522** (2012) 30.
- [34] W. Yao and J. Ye, *J. Phys. Chem. B* **110** (2006) 11188.
- [35] S. Dutta, S. Som and S. Sharma, *Dalton T.* **42** (2013) 9654.
- [36] K. G. Sharma and N. R. Singh, *New J. Chem.* **37** (2013) 2784.
- [37] B. Singh, A. Parchur, R. Ningthoujam, A. Ansari, P. Singh and S. Rai, *Dalton T.* **43** (2014) 4779.
- [38] A. K. Parchur, R. S. Ningthoujam, S. B. Rai, G. S. Okram, R. A. Singh, M. Tyagi, S. Gadkari, R. Tewari and R. K. Vatsa, *Dalton T.* **40** (2011) 7595.
- [39] G. Liu and B. Jacquier, "Spectroscopic properties of rare earths in optical materials" Springer,(2006).
- [40] J. Liao, D. Zhou, X. Qiu, S. Liu and H. Wen, *Optik* **124** (2013) 5057.
- [41] M. Puchalska, E. Zych, M. Sobczyk, A. Watras and P. Deren, *Mater. Chem. Phys.* **147** (2014) 304.
- [42] S. Shi, J. Gao and J. Zhou, *Opt. Mater.* **30** (2008) 1616.

- [43] B. D. Cullity and S. R. Stock, "Elements of X-ray diffraction" Pearson,(2001).
- [44] G. Williamson and W. Hall, *Acta Metallurgica* **1** (1953) 22.
- [45] P. Ghosh, J. Oliva, E. D. I. Rosa, K. K. Haldar, D. Solis and A. Patra, *J. Phys. Chem. C* **112** (2008) 9650.
- [46] S. Zhang, Y. Hu, L. Chen, X. Wang, G. Ju and Y. Fan, *J. Lumin* **142** (2013) 116.
- [47] X. He, M. Guan, N. Lian, J. Sun and T. Shang, *J. Alloy. Compd.* **492** (2010) 452.
- [48] C. Kodaira, H. Brito, O. Malta and O. Serra, *J. Lumin* **101** (2003) 11.
- [49] N. S. Singh, R. Ningthoujam, M. N. Luwang, S. D. Singh and R. Vatsa, *Chem. Phys. Lett.* **480** (2009) 237.
- [50] M. Aumer, S. LeBoeuf, S. Bedair, M. Smith, J. Lin and H. Jiang, *Appl. Phys. Lett.* **77** (2000) 821.
- [51] Z. Zhang, H. Chen, X. Yang and J. Zhao, *Mater. Sci. Eng. B* **145** (2007) 34.
- [52] R. Pode and S. Dhoble, *Physica Status Solidi (B)* **203** (1997) 571.
- [53] Y. Porter-Chapman, E. Bourret-Courchesne and S. E. Derenzo, *J. Lumin* **128** (2008) 87.

감사의 글

2년이라는 석사과정 시간이 쏠살같이 지나가고 부족한 것이 많은 제가 이렇게 졸업논문을 작성하기까지 많은 도움을 주신 모든 분들에게 감사의 마음을 전하고자 합니다. 우선 저를 이 자리에 있게 해주시고 지도해주신 정중현 교수님께 깊이 감사드립니다. 힘들어 하는 저에게 아낌없는 지원과 관심을 주시고 연구할 수 있게 해주셔서 감사합니다.

학문적으로 많은 가르침을 주시고 논문을 완성하기까지 많은 지도를 해주신 동의대 김종환 교수님과 언제나 유쾌한 즐거움을 주시고 연구에 많은 관심과 조언을 아끼지 않으신 문병기 교수님께도 감사의 말씀을 드립니다. 그리고 인자한 미소로 응원해주신 최병춘 교수님, 학부 때부터 지켜봐 주시고 따뜻한 한 끼와 함께 애정과 격려를 아낌없이 주셨던 최점수 교수님께 진심으로 감사드립니다.

대학원 생활을 하는 동안 저의 부족한 부분을 채워주시고 아낌없이 조언해주신 심규성 박사님, 연구실 선배로서 오랜 시간을 함께 하지는 못했지만 조언과 충고를 아낌없이 해주신 정종원 선배님, 박성욱 선배님께 감사드립니다. 그리고 바쁘신 와중에 막힐 때 마다 조언을 해주신 박진영 선배님, 졸업하셨지만 함께 연구하고 도와주신 권숙현 선배님께도 감사합니다.

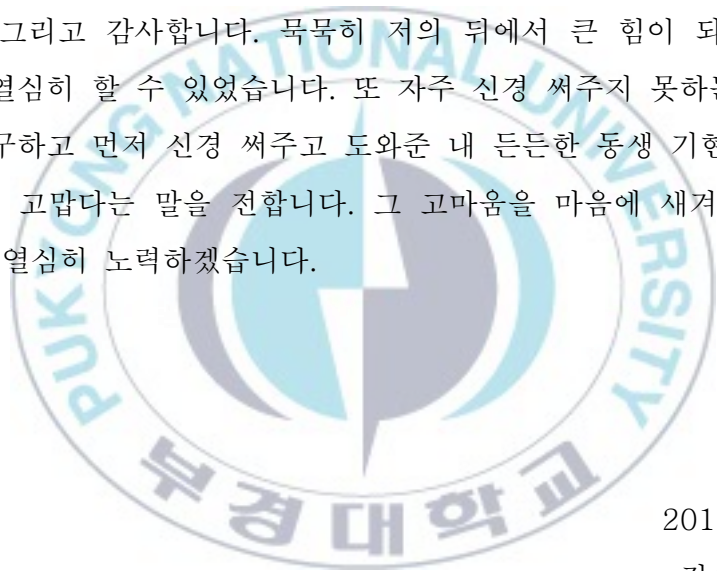
낮도 가리고 힘들어하는 저를 잘 챙겨주신 연우 언니와 현미 언니께도 정말 감사합니다. 힘들고 지칠 때마다 옆에 있어주시고 나서서 도와주시고, 힘든 대학원 생활에 많은 추억을 함께해주셔서 감사드립니다. 입학해서 논문 준비하기까지 함께 해주고 도와준 동기 오주현, 똑똑한 Wang LiLi, Guo Yue에게도 고맙다고 전하고 싶습니다.

결코 짧지 않았던 시간 동안 바쁜 저를 이해해주고 챙겨주고 신경 써준 보실이에게도 미안하면서 고맙다고 전하고 싶고, 학교생활을 함께 하면서 외롭지 않게 해준 동기 현정이, 상혁이, 선배보다는 언니처

럼 챙겨주시고 아껴주신 해랑 언니, 비록 떨어져있지만 늘 먼저 연락 해주고 신경 써준 재현이 고맙습니다. 먼 타지에서 지내고 있는 저를 위해 찾아오고 격려해준 내 친구들 아영이, 희정이, 미영이 정말 고맙다고 전하고 싶습니다.

미처 언급하지는 못했지만 논문을 완성하기까지 힘들고 지칠 때마다 제 주변에서 격려와 응원을 해주신 많은 고마운 분들의 도움이 있었기에 무사히 여기까지 올 수 있었습니다. 정말 감사드립니다.

마지막으로 언제나 저의 선택을 믿고 지지해 주신 부모님 정말 사랑합니다. 그리고 감사합니다. 묵묵히 저의 뒤에서 큰 힘이 되어주셔서 이렇게 열심히 할 수 있었습니다. 또 자주 신경 써주지 못하는 누나임에도 불구하고 먼저 신경 써주고 도와준 내 든든한 동생 기현이, 수빈이에게도 고맙다는 말을 전합니다. 그 고마움을 마음에 새겨 잊지 않고 더욱 열심히 노력하겠습니다.



2015년 7월
김은옥 올림